Article

Cell Systems

Frequency Modulation of Transcriptional Bursting Enables Sensitive and Rapid Gene Regulation

Graphical Abstract

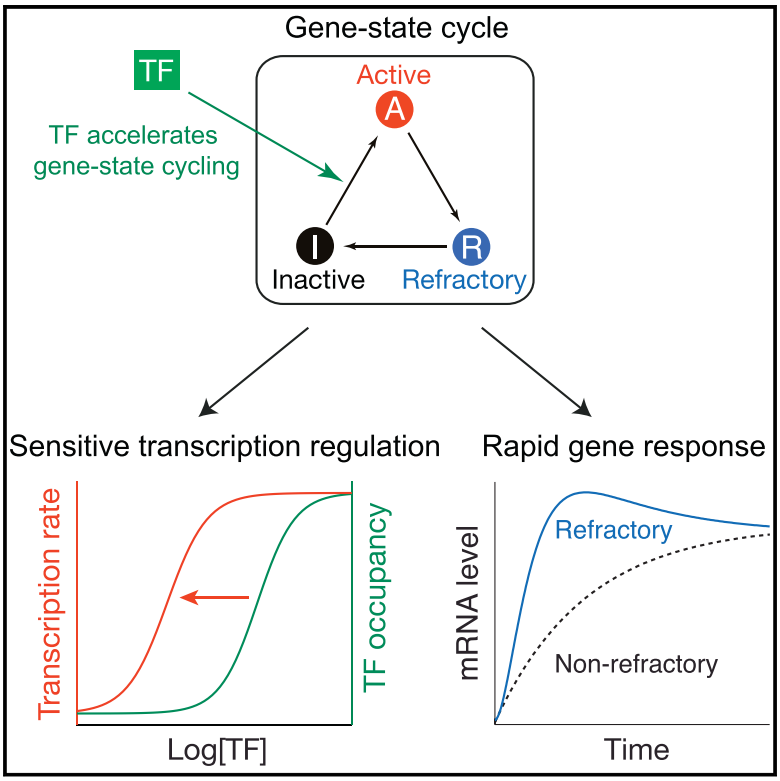

Authors

Congxin Li, François Cesbron, Michael Oehler, Michael Brunner, Thomas Höfer

Correspondence

michael.brunner@bzh.uni-heidelberg.de (M.B.), t.hoefer@dkfz.de (T.H.)

In Brief

Quantitating how transcription factors act on the transcriptional bursting cycle provides a non-equilibrium framework for the study of gene regulation. Transcription factors that increase transcription burst frequency allow for sensitive and rapid gene regulation.

Highlights

- We construct gene-regulatory functions based on the transcriptional bursting cycle
- Promoter refractoriness enables rapid and precise transcription responses to stimuli
- Transcription responds sensitively to transcription factors modulating burst frequency
- Genes with inherently different activation rates are differentially regulated by a TF

Li et al., 2018, Cell Systems 6, 409–423
April 25, 2018
https://doi.org/10.1016/j.cels.2018.01.012

CellPress

Cell Systems
Article

Frequency Modulation of Transcriptional Bursting Enables Sensitive and Rapid Gene Regulation

Congxin Li,[1,2,4] François Cesbron,[3,4] Michael Oehler,[3] Michael Brunner,[3,*] and Thomas Höfer[1,2,5,*]
[1]Division of Theoretical Systems Biology, German Cancer Research Center (DKFZ), 69120 Heidelberg, Germany
[2]Bioquant Center, Heidelberg University, 69120 Heidelberg, Germany
[3]Biochemistry Center, Heidelberg University, 69120 Heidelberg, Germany
[4]These authors contributed equally
[5]Lead Contact
*Correspondence: michael.brunner@bzh.uni-heidelberg.de (M.B.), t.hoefer@dkfz.de (T.H.)
https://doi.org/10.1016/j.cels.2018.01.012

SUMMARY

Gene regulation is a complex non-equilibrium process. Here, we show that quantitating the temporal regulation of key gene states (transcriptionally inactive, active, and refractory) provides a parsimonious framework for analyzing gene regulation. Our theory makes two non-intuitive predictions. First, for transcription factors (TFs) that regulate transcription burst frequency, as opposed to amplitude or duration, weak TF binding is sufficient to elicit strong transcriptional responses. Second, refractoriness of a gene after a transcription burst enables rapid responses to stimuli. We validate both predictions experimentally by exploiting the natural, optogenetic-like responsiveness of the *Neurospora* GATA-type TF White Collar Complex (WCC) to blue light. Further, we demonstrate that differential regulation of WCC target genes is caused by different gene activation rates, not different TF occupancy, and that these rates are tuned by both the core promoter and the distance between TF-binding site and core promoter. In total, our work demonstrates the relevance of a kinetic, non-equilibrium framework for understanding transcriptional regulation.

INTRODUCTION

How transcription factors (TFs) quantitatively control the rate of transcription has been a central question of molecular biology. The relation between TF concentration and transcription rate is termed the gene-regulatory function (Rosenfeld et al., 2005; Setty et al., 2003), and classical theory emphasizes TF occupancy of *cis*-regulatory DNA elements as a proxy for transcription rate (Ptashne and Gann, 2002). However, how context-specific, differential activation of target genes is achieved remains a fundamentally unresolved problem, as TFs bind to short (~10 bp) DNA sequences with considerable degeneracy (Spitz and Furlong, 2012). Sophisticated models, considering binding of multiple TFs, interactions of TF with nucleosomes, and number of binding sites, have been devised to account for specificity (Bintu et al., 2005; Segal et al., 2008; Giorgetti et al., 2010; Teif et al., 2013). A common denominator of these models is that they compute equilibrium distributions for the binding of TFs and their interaction partners. However, research in the last decade has profoundly changed this "equilibrium view" of transcriptional regulation in eukaryotes by showing that TFs do not only serve as docking sites for the general transcription machinery, but recruit enzymes that catalyze transitions between chromatin states (Lefstin and Yamamoto, 1998; Coulon et al., 2013; Voss and Hager, 2014). In particular, TF-induced nucleosome remodeling, possibly in concert with covalent modifications of histones, appears to be rate limiting for transcriptional activation (Boeger et al., 2008; Kim and O'Shea, 2008). Thus TFs may impart memory of their presence to the chromatin state, obviating the need for continuous binding (Voss et al., 2011). Collectively, these findings challenge the view that the transcriptional machinery decodes TF activity based solely on the degree of TF occupancy.

Stimulated by these experimental observations, a new class of "non-equilibrium" models of gene regulation has begun to be developed (Ahsendorf et al., 2014; Estrada et al., 2016; Scholes et al., 2017). The defining feature of these models is the presence of dynamic transitions between gene states, characterized both by TF binding and chromatin configuration; similar concepts have been developed for DNA repair (Luijsterburg et al., 2010; Verbruggen et al., 2014). Estrada et al. (2016) proposed a model that shows with considerable generality that gene regulation out of equilibrium may breach a regulatory "barrier" for the shape of the gene-regulation function inherent in equilibrium-binding models. Closer to experiment, Scholes et al. (2017) modeled molecular states of the general transcription cycle and identified possibilities for the kinetic control of combinatorial gene regulation. However, specific experimental support for predicted non-equilibrium mechanisms of decoding TF activity has so far been lacking.

Here we develop a family of non-equilibrium models of gene regulation with the purpose of confronting generic theory with quantitative experimental data. Our starting point is the observation that transcription often occurs in episodic bursts of mRNA production separated by silent intervals, rather than as a Poissonian process during which transcripts accumulate at a constant rate. Genes with Poissonian transcript noise have also been described (Battich et al., 2015), especially after correcting for confounding parameters such as cell size (Ietswaart et al., 2017). However, transcriptional bursting has been widely

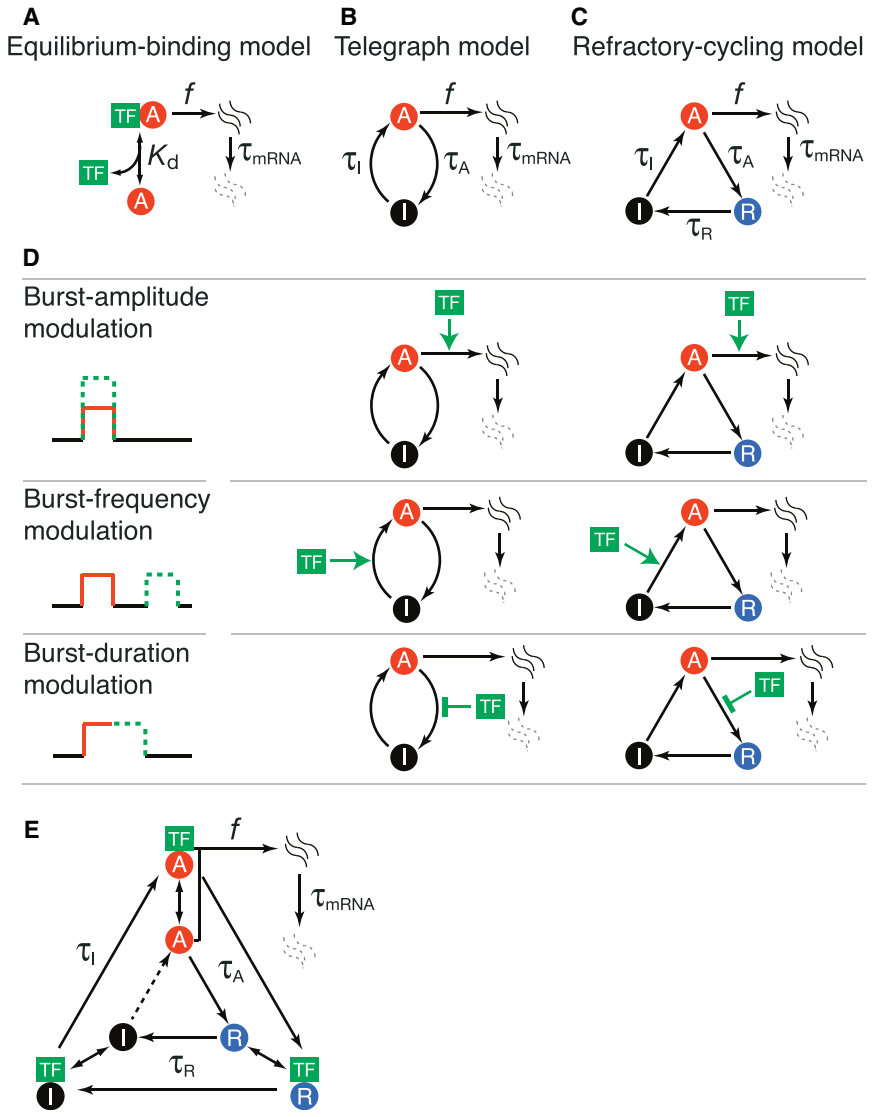

Figure 1. A Family of Non-equilibrium Models for Transcriptional Regulation

(A) Equilibrium-binding model, (B) telegraph model, and (C) refractory-cycling model.

(D) A TF may activate gene expression through modulation of transcription burst amplitude, frequency or duration.

(E) An example of detailed scheme for the refractory-cycling model with TF modulating the burst frequency (for all models see Figure S1).

identified and characterized for eukaryotic (and also many bacterial) genes (Raj and van Oudenaarden, 2008; Hornung et al., 2012; Sanchez and Golding, 2013; Nicolas et al., 2017).

The dynamics of transcriptional bursting imply, in turn, the existence of long-lived gene states, which can chiefly be characterized as transcriptionally inactive (but activatable), active, and refractory (Harper et al., 2011; Suter et al., 2011; Zechner et al., 2014; Zoller et al., 2015). Cesbron et al. (2015) have recently shown that transcriptional refractoriness is a property of the core promoter, by utilizing a natural "optogenetic" system: blue-light-controlled transcription in the fungus *Neurospora crassa*. The ubiquity of transcriptional bursting suggests that generic models of transcription dynamics may be based on quantifying the transitions between key long-lived gene states in the bursting cycle. Indeed, transcriptional modulators (TFs or drugs altering chromatin state) affect the average frequency or/and size of transcription bursts (Dar et al., 2012; Larson et al., 2013; Molina et al., 2013; Neuert et al., 2013; Senecal et al., 2014).

Here we demonstrate that the mechanisms by which TFs modulate the dynamics of transcriptional bursting shape the gene-regulatory function. We ask how sensitively and how rapidly a gene responds to a TF, and how differential expression could be encoded in dynamic properties of the bursting cycle. The theory predicts that speed and sensitivity of a gene's response overcome theoretical limits of conventional equilibrium binding models. We obtain quantitative experimental evidence for the validity of the predictions, using light-controlled transcription in *Neurospora*.

RESULTS

Modulators of Transcription Burst Frequency Sensitively Regulate Transcript Abundance

We begin by constructing a family of generic models for the action of TFs (Figure 1). In the most basic model, transcriptional activators recruit RNA polymerase (Ptashne and Gann, 2002), with the activator occupancy at its regulatory site(s) determining the rate at which polymerase initiates transcription (*f*) (*equilibrium-binding model*, Figure 1A). At constant TF concentration, the distribution of transcript numbers in this model is Poissonian. The simplest model that produces transcriptional bursting is the *random telegraph model* (Peccoud and Ycart, 1995; Friedman et al., 2006), with the gene switching between an inactive state and an active state from which several rounds of transcription initiation might take place (Figure 1B). Statistical inference from single-cell time series of gene expression in yeast has favored this model (Zechner et al., 2014). In mammalian cells (Harper et al., 2011; Suter et al., 2011) and *Neurospora* (Cesbron et al., 2015), the bursting cycle of gene promoters has been found to contain a state that is refractory to activation. The simplest model accounting for these observations is the three-state *refractory-cycling model* (Figure 1C), although further gene states with appreciable lifetime may exist (Zoller et al., 2015).

Random telegraph and refractory-cycling models allow for three distinct modes of regulation: modulation of the amplitude of a transcription burst (amplitude modulation [AM]), burst

frequency modulation (FM), and modulation of burst duration (DM) (Figure 1D). TFs recruiting RNA polymerase will enhance the rate of transcription initiation in the active gene state, *f*, and thus control transcription burst amplitude (AM). TFs recruiting chromatin-modifying enzymes will cause the transition of the gene from an inactive into a transcriptionally active state, e.g., by nucleosome remodeling. Such activators will shorten the lifetime of the inactive gene state, τ_I, and thus modulate burst frequency (FM). Frequency modulation may also occur if an activator shortens the duration of the refractory state τ_R (this case is discussed in the STAR Methods, Mathematical Modeling, Figure S1). Finally, it is conceivable that a TF counteracts promoter inactivation, prolonging the lifetime of the active state τ_A and hence burst duration (DM). Depending on its interaction partners, a given TF might act through more than one mode on transcription (Figure S1).

The properties of the gene-regulatory function (viewed in its usual "macroscopic" sense as the population average of transcript number versus TF concentration) are shaped by the "microscopic" modes of decoding TF activity: AM, FM, or DM. To show this, we focus on the case of a single TF driving transcription from a *cis*-regulatory element. For simplicity, we assume that the TF may bind to each of the gene states in the telegraph or refractory-cycling models and functions as an activator in a specific state. As an example, the refractory-cycling model with frequency modulation is shown in Figure 1E. Promoter activation proceeds with a low basal rate in the absence of bound TF (dashed line from state I to state A) and is strongly enhanced after TF binding (solid line); all other transitions proceed at equal rates with or without bound TF. Similarly, for AM or DM, we made the respective regulated processes in the models dependent on the presence of the TF (Figure S1; STAR Methods, Mathematical Modeling).

The TF occupancy of the *cis*-regulatory element is a saturating function of TF concentration, [TF], being half-maximal at [TF] = K_D, the dissociation constant (Figure 2A). To understand how the gene-regulatory function, transcription rate *v* versus [TF], depends on [TF], we calculated the steady-state transcription rates of the AM, FM, and DM random telegraph and refractory-cycling models. For all models, the gene-regulatory function saturates with increasing [TF] (akin to the Michaelis-Menten equation for enzyme kinetics):

$$v = v_{max}\frac{\beta + [TF]}{\Omega + [TF]}, \qquad \text{(Equation 1)}$$

with the maximal transcription rate v_{max} and the operating point (half-saturation constant), Ω; β is due to the basal transcription rate in the absence of TF and is smaller than Ω (Box 1). For the simple equilibrium-binding model, the same expression holds with $\Omega = K_D$, and hence the gene-regulatory function of this model is proportional to TF occupancy (Figure 2B, upper panel). By contrast, the operating point in the non-equilibrium models is also a function of the lifetimes of the gene states in the bursting cycle $\Omega = \Omega(\tau_I, \tau_A, \tau_R, K_D)$ (Box 1). As a consequence, the gene-regulatory function is generally not proportional to TF occupancy. There are three principal cases:

- The bound TF accelerates a transition in the transcriptional bursting cycle. For an activator, this would be the Inactive-to-Active transition (or the Refractory-to-Inactive transition), causing burst frequency modulation. Then the transcriptional output becomes maximal already before TF occupancy saturates, as the operating point of the gene-regulatory function is smaller than the TF dissociation constant, $\Omega_{FM} < K_D$ (Figure 2B, orange line).
- The bound TF inhibits a transition in the bursting cycle. For an activator, this would be the Active-to-Inactive transition (random telegraph model) or the Active-to-Refractory transition (refractory-cycling model), thus prolonging burst duration (DM). Then the transcription rate responds much less sensitively to the concentration of the activator and increases only when the response element already shows strong occupancy ($\Omega_{DM} > K_D$ Figure 2B, cyan line).
- The bound TF leaves the bursting cycle dynamics unaffected but changes the transcription initiation rate from the active promoter (AM). Only in this case is the transcriptional output proportional to TF occupancy ($\Omega_{AM} = K_D$ Figure 2B, black line).

Thus a TF accelerating (slowing) the transcriptional bursting cycle has an operating point that is smaller (larger) than its dissociation constant K_D. These effects arise because the TFs regulate the lifetime of specific states in the non-equilibrium bursting cycle. In the case of FM, the TF in question triggers the Inactive-to-Active transition but is not needed to maintain the active state, hence weak TF occupancy suffices for achieving maximal transcription rate. Conversely, in the case of DM, the TF inhibits the Active-to-Refractory/Inactive transition, working against a constant slippage of the inactivating transition taking place. Therefore, very high TF occupancy is needed to shut down inactivation (see Box 1 for details). Notably, transcription responds to a TF that modulates burst frequency more sensitively ($\Omega_{FM} < K_D$) than to a factor recruiting RNA polymerase (for which $\Omega_{AM} = \Omega_{EQ} = K_D$); burst frequency modulation thus overcomes a sensitivity limit inherent in the equilibrium-binding binding model. Of note, this conclusion remains valid for responses to transient stimuli (Figure S2), as well as an arbitrary number of refractory states in the bursting cycle (Figure S1A; STAR Methods, Mathematical Modeling; Zoller et al., 2015).

For the subsequent analysis of experimental data, the case of a TF modulating burst frequency by accelerating the Inactive-to-Active transition will be most relevant. Then the operating point is:

$$\Omega_{FM} = K_D\frac{\tau_I}{\tau_I + \tau_A + \tau_R} < K_D, \qquad \text{(Equation 2)}$$

that is, K_D is weighted by the TF-bound fraction of genes in the inactive state (for simplicity, basal transcription was set to zero, see Box 1 for the general case). Equation 2 entails a specific prediction. If a gene is readily activated upon binding of the TF (τ_I small), it should be sensitive to even small [TF] and, hence, weak occupancy of its response element ($\Omega_{FM} \ll K_D$). By contrast, if a gene requires a long time for activation (τ_I large), it needs higher [TF] for activation and may even approach the equilibrium limit ($\Omega_{FM} \sim K_D$) (Figure 2C). In summary, the theory predicts that (1) a gene may respond very sensitively to an activator that modulates burst frequency, and (2) that the respective

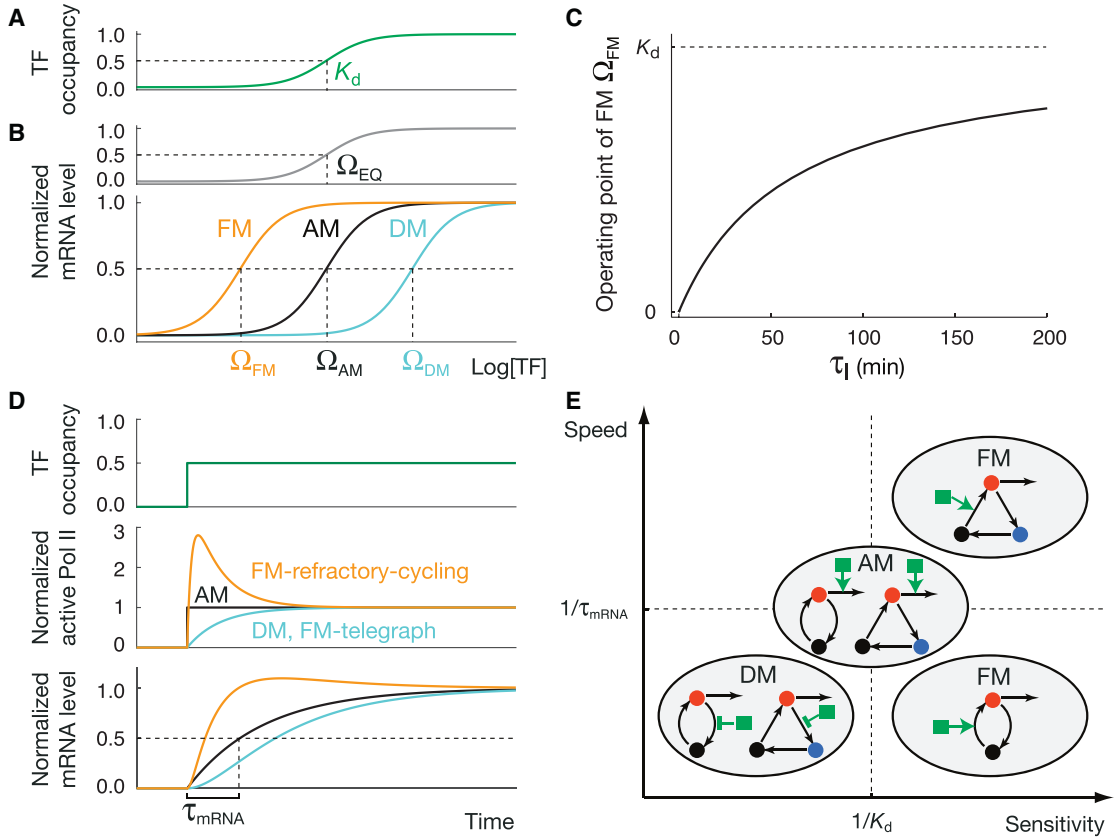

Figure 2. Theoretical Predictions from the Generic Models of Transcriptional Regulation

(A) Steady-state TF occupancy as a saturating function of TF concentration.

(B) Dose responses of steady-state mRNA levels (normalized to maximum) for equilibrium-binding model (EQ, gray line), and non-equilibrium models with AM (black line), DM (cyan line), and FM (orange line); telegraph and refractory-cycling models have principally the same behavior of the dose responses. The operating point Ω is defined as the TF concentration at which the mRNA level reaches half saturation.

(C) The operating point of FM model as a function of the lifetime of the inactive promoter state τ_I.

(D) In response to a sudden increase in TF binding (upper panel) the different models show distinct dynamics of promoter activity (middle panel) and mRNA output (bottom panel). Notably, transcription rate in the FM refractory-cycling model overshoots.

(E) Graphical summary of the theoretical predictions. Parameter values: $\tau_I = 1$ min, $\tau_A = 15$ min and $\tau_R = 40$ min for the FM refractory-cycling model (cf. Table S2 for experimentally inferred values) and $\tau_I = 15$ min, $\tau_A = 1$ min, $\tau_R = 40$ min for the DM refractory-cycling model; mRNA lifetime in (D) is 30 min. See also Figures S2–S4 and Table S1.

operating point is controlled by the gene's activation rate: a kinetic property of the bursting cycle.

Refractory Genes Can Be Induced Rapidly

Next, we asked how fast transcript levels rise in response to an activator. The kinetics of transcription initiation, elongation/splicing, and mRNA loss will all affect the speed of the response to some degree. As a general principle, the time for switching on a molecular component in a simple, monotonic manner is determined by the lifetime of the component, and hence mRNA lifetime is expected to limit the speed of the transcriptional response to a stimulus (Savageau, 1974; Rosenfeld et al., 2002; Alberts et al., 2015). In particular, transcript and protein lifetimes cannot be arbitrarily short if a certain steady-state level is to be achieved.

We systematically investigated the kinetic responses of the different models and found that in the majority of cases (AM and DM in both telegraph and refractory-cycling models, FM in the telegraph model), mRNA lifetime limits the speed of the response (Figure 2D, black lines and cyan lines; STAR Methods, Mathematical Modeling). In all these models, a rise in TF activity leads to a monotonic increase in transcription rate until the steady state is reached. The resulting rise in mRNA level trails the increase in promoter activity with a delay that is governed by mRNA lifetime. In particular, increasing the rate of gene activation in the model would not speed up the response time to steady state because the steady-state level would also increase.

By contrast, frequency modulation in the refractory-cycling model shows a fundamentally different response, because response speed and steady state can be decoupled due to the additional degree of freedom provided by the refractory state. To illustrate this, we consider the simple case that the basal transcription rate vanishes in the absence of TF; TF is activated at a given time point and then held constant. Prior to TF activation, the steady state of the model is full occupancy of the inactive state. If, after TF binding, the gene activation rate is large,

Box 1. Gene-Regulatory Functions for Transcriptional Bursting Models

The population-level dynamics of the random telegraph and refractory-cycling models are described by systems of ordinary differential equations for the fractions of genes in the inactive, active and (for refractory cycling) refractory states, being TF bound or unbound. We calculated the gene-regulatory functions in terms of the steady-state transcription rates for constant [TF] (STAR Methods, Mathematical Modeling) and discuss them in turn for AM, FM, and DM.

In the case of AM, the binding of the TF does not affect the transcriptional bursting cycle but rather enhances the initiation rate from the active state. Let τ_A, τ_I, and τ_R be the average lifetimes of the active, inactive, and refractory gene states (for the random telegraph model $\tau_R = 0$). Further, let K_D and f denote, respectively, the dissociation constant of the TF and the transcription initiation rate with TF bound. Without bound TF, transcription is initiated with the basal rate $\varepsilon_{AM}f$, where $0 \leq \varepsilon_{AM} < 1$. The gene-regulatory function is

$$\nu_{AM} = \underbrace{f\frac{\tau_A}{\tau_I+\tau_A+\tau_R}}_{\text{maximal rate}}\underbrace{\frac{\varepsilon_{AM}K_D+[TF]}{K_D+[TF]}}_{\text{dose response}}. \quad \text{(Equation 4)}$$

The operating point is defined as the [TF] at which the transcription rate is halfway between the basal and maximal rates, yielding

$$\Omega_{AM} = K_D. \quad \text{(Equation 5)}$$

Hence the dose response of the AM model is identical to the basic equilibrium-binding model. We will see below that this is due to the fact that the bursting cycle is not influenced by TF binding. The maximal transcription rate,

$$\nu_{max} = f\frac{\tau_A}{\tau_I+\tau_A+\tau_R}, \quad \text{(Equation 6)}$$

is the product of the occupancy of the active gene state and the initiation rate.

For the FM and DM models, the bursting cycle is modulated by TF binding. Therefore, we distinguish basal (TF unbound) and activated (TF bound) bursting cycles. In the FM model, bound TF accelerates the transition from the inactive to the active gene state. We denote the lifetime of the inactive gene state in the presence of bound TF by τ_I (active bursting cycle) and in the absence of TF by τ_I/ε_{FM}, where $0 \leq \varepsilon_{FM} < 1$ (basal bursting cycle). The gene-regulatory function has the same principal form as for AM,

$$\nu_{FM} = \nu_{max}\frac{\varepsilon_{FM}K_D+[TF]}{\Omega_{FM}+[TF]}, \quad \text{(Equation 7)}$$

with identical maximal rate but different dose response, as the operating point is

$$\Omega_{FM} = K_D\frac{\tau_I+\varepsilon_{FM}(\tau_A+\tau_R)}{\tau_I+\tau_A+\tau_R} < K_D. \quad \text{(Equation 8)}$$

For DM, we denote the lifetime of the active state with bound TF by τ_A (activated bursting cycle) and in the absence of TF by $\varepsilon_{DM}\tau_A$, where $0 < \varepsilon_{DM} < 1$ (basal bursting cycle). The gene-regulatory function becomes

$$\nu_{DM} = \nu_{max}\frac{K_D+[TF]}{\Omega_{DM}+[TF]}, \quad \text{(Equation 9)}$$

with the operating point

$$\Omega_{DM} = K_D\frac{\tau_A+(\tau_I+\tau_R)/\varepsilon_{DM}}{\tau_I+\tau_A+\tau_R} > K_D. \quad \text{(Equation 10)}$$

Thus the essential difference between the gene-regulatory functions for AM, FM, and DM is in the operating point. Remarkably, the operating points for the distinct models follow from a general relation. Let $R_{active,i}$ and $R_{basal,i}$ denote the fractions of time that gene state i (i = A, R, I) occupies in the active and basal bursting cycles. Consider the gene state whose lifetime is regulated by the binding of the TF. For FM, we have i = I and

$$R_{active,I} = \frac{\tau_I}{\tau_I+\tau_A+\tau_R} \text{ and } R_{basal,I} = \frac{\tau_I/\varepsilon_{FM}}{\tau_I/\varepsilon_{FM}+\tau_A+\tau_R}, \quad \text{(Equation 11)}$$

while for DM, we have i = A, and

(Continued on next page)

Box 1. *Continued*

$$R_{\text{active,A}} = \frac{\tau_A}{\tau_I + \tau_A + \tau_R} \text{ and } R_{\text{basal,A}} = \frac{\tau_A \varepsilon_{DM}}{\tau_I + \tau_A \varepsilon_{DM} + \tau_R} . \quad \text{(Equation 12)}$$

It is straightforward to verify that the operating point is, in general,

$$\Omega = \frac{R_{\text{active},i}}{R_{\text{basal},i}} K_D, \quad \text{(Equation 13)}$$

where the index i denotes the regulated gene state. This equation also contains the AM case, as here TF-bound and unbound cycles have the same length and, hence, $R_{\text{active},i}/R_{\text{basal},i} = 1$. Moreover, Equation 13 also holds in the relevant limiting case of vanishing basal cycle rate for FM ($\varepsilon_{FM} = 0$), as the fraction occupied by the inactive state is 1.

These arguments can be phrased more generally, considering multiple refractory states and also TFs acting as repressors (STAR Methods, Mathematical Modeling). A TF enhancing the Inactive-to-Active transition is an example of a TF accelerating the transcriptional burst cycle when bound. For such "accelerating" TFs, we always have $\Omega < K_D$. Conversely, a TF extending the lifetime of the active state is an example of prolongation of the bursting cycle by the bound TF. Such "braking" TFs always have $\Omega > K_D$. These cases include repressor action, e.g., when a TF shortens the lifetime of the active state or extends the lifetime of the inactive or refractory states; the dose response is then a decreasing function of [TF], but the operating point is nevertheless determined by Equation 13 (STAR Methods, Mathematical Modeling). Finally, a TF that leaves the lifetime of the bursting cycle unchanged has $\Omega = K_D$. Thus, the operating point of the gene-regulatory function is shaped by the non-equilibrium nature of the transcriptional bursting cycle.

transcript will start to accumulate rapidly. However, the steady state to which the system relaxes could still be low, as a long-lived refractory state would prevent immediate reactivation of transcription. In this situation, the transcription rate overshoots (on the population level) before settling to the steady state (Figure 2D, orange lines). As a consequence, mRNA levels may rise rapidly, overshoot, and relax to the steady state. If transcription rate overshoots, the response time is no longer limited by mRNA lifetime (Figure S3; STAR Methods, Mathematical Modeling). Thus, paradoxically, the theory predicts that transcriptional refractoriness allows for rapid induction of transcript. Moreover, we find that the amplitude of the transcriptional response is insensitive to the duration of the input stimulus, thus allowing for robust, stereotypic gene induction once a stimulus threshold is crossed (Figure S4).

Taken together, the theory predicts that the decoding of TF activity by transcription bursting cycles overcomes principal limits inherent in equilibrium-binding models (Figure 2E): strong transcription responses may be induced without saturating the occupancy of TF binding sites, and gene refractoriness allows for a rapid rise in transcript levels that is not limited by transcript lifetime.

Light-Controlled Genes of *Neurospora* Are Frequency Modulated

We tested the utility of the models for understanding experimental data. To this end, we made use of the light-controlled GATA-type TF, White Collar Complex (WCC), in *Neurospora crassa*. Activation of WCC by blue light is based on a stable covalent photoadduct between the TF and its bound flavin adenine dinucleotide cofactor (Malzahn et al., 2010). Hence, a brief non-saturating pulse of blue light splits the population of WCC into an activated fraction and an inactive fraction, which is available for activation by a consecutive light pulse. After a brief light pulse, activated WCC binds to the *cis*-regulatory elements of its target genes, the light-response elements (LREs), and synchronously activates their transcription in this syncytial organism. As we have shown recently (Cesbron et al., 2015), double light pulses reveal the existence of transcriptional refractoriness (depicted schematically in Figure 3A, upper panel). WCC target genes show a continuum of responses in this experimental setting, ranging from clearly refractory genes, such as *frequency* (*frq*), to genes with no apparent refractoriness, such as *vivid* (*vvd*) (Figure 3A, lower panel).

To test our theory against experiment we used a comprehensive, time-resolved dataset obtained for *frq* and *vvd*, consisting of measurements on WCC binding (by chromatin immunoprecipitation-PCR), mRNA levels (by RT-PCR), and protein levels (measured with a stably integrated luciferase reporter construct) for single and double-light-pulse protocols (Cesbron et al., 2015). To fit the models to these data, we modeled the light-induced activation and subsequent inactivation of the WCC and coupled it to all possible telegraph or refractory-cycling models for *frq* and *vvd* expression showing AM, FM, or DM, or combinations of these decoding modes (Figures S1 and S5A). This yielded 484 distinct models that share the WCC activation pulse but, for each gene, allow different numbers of states (telegraph or refractory-cycling models) and activation modes by WCC (STAR Methods, Mathematical Modeling). To comprehensively scan the space of the ~30 model parameters, we performed 1,000 optimization runs for each of these models, using Latin hypercube sampling for the initial conditions. We then ranked the models according to their performance in reproducing all the data by two standard criteria, the Akaike information criterion (Akaike, 1974) and the goodness of fit (Figures 3B and S5B). Both criteria yielded a clear partitioning of the models into a small group consisting of four models that account for the data and the large remainder that does not (Figure 3C). This result indicates that, at the given level of model complexity, the experimental data are highly informative on the underlying gene-regulatory mechanisms.

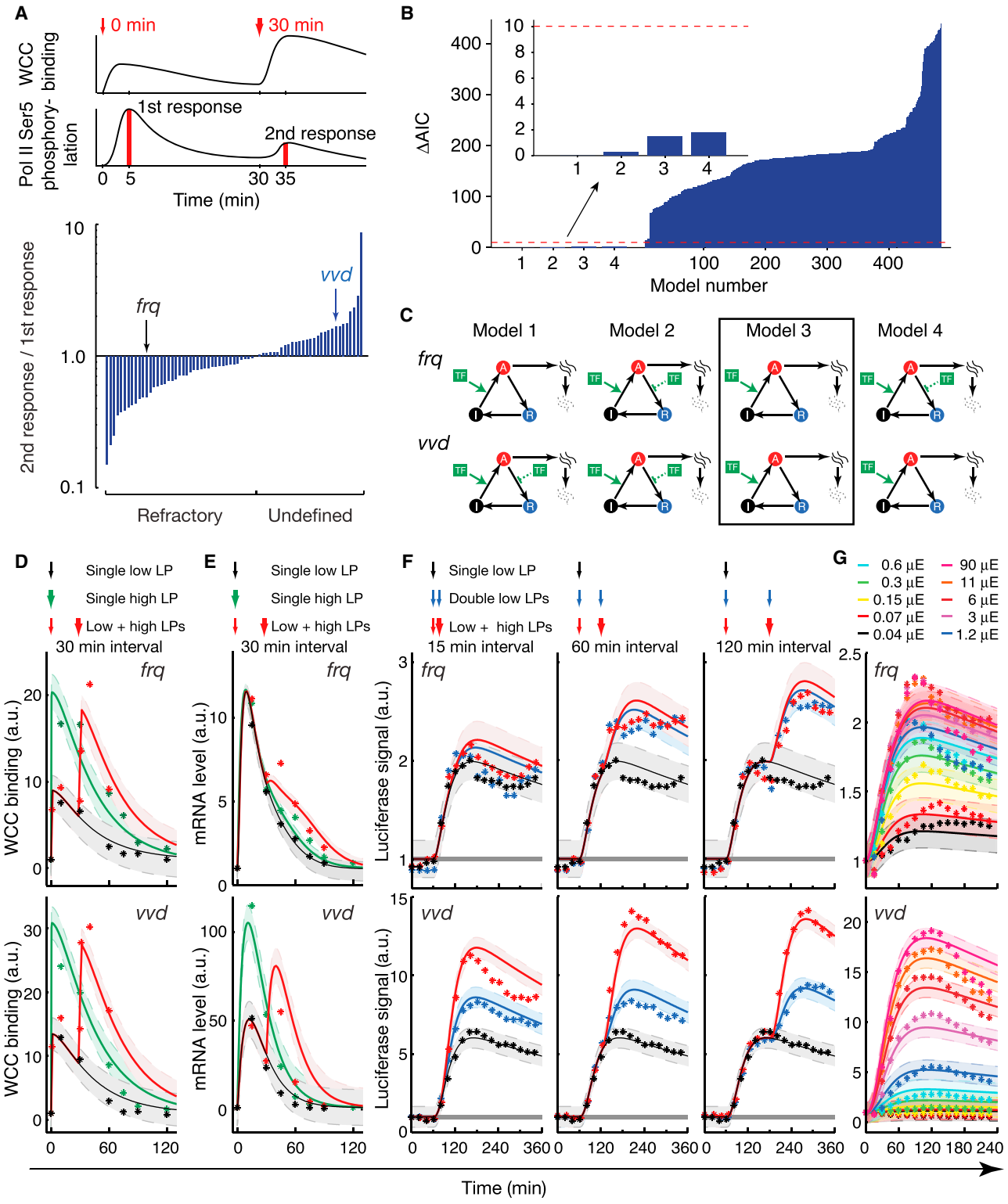

Figure 3. Model Selection and Parameter Inference for Light-Controlled Gene Activation in *Neurospora crassa*

(A) Repeated light pulses reveal a refractory gene state: the light-activated TF WCC is recruited to its regulatory elements (LREs) by each light pulse, yet transcription is refractory during the second pulse (upper panel, schematic drawing based on data of Cesbron et al., 2015); response ratio to second versus first light pulse (given 30 min apart) for 71 light-inducible genes, as quantified by the recruitment of Ser5-phosphorylated RNA polymerase (lower panel, redrawn from Cesbron et al., 2015).

(legend continued on next page)

The fitting models are variations on a common theme: they all include a refractory state for both *frq* and *vvd*, and burst frequency modulation by WCC (Figure 3C). Thus, the large-scale model selection identified a common mechanism for the regulation of WCC target genes: frequency modulation of a transcriptional bursting cycle with a refractory period. The inferred role of WCC in bringing the genes into an active state is supported by its involvement in chromatin remodeling (Sancar et al., 2015).

We selected the most parsimonious Model 3, which has no additional features for further analysis in the remainder of the paper (the other three models effectively converge to Model 3 given the inferred parameter values). For both *vvd* and *frq*, the model captured the dynamics of WCC binding to the respective LREs (Figure 3D), as well as the dynamics of mRNA level (Figure 3E) and luciferase reporter (Figure 3F) in single- and double-pulse experiments. Moreover, comprehensive dose responses, where active WCC levels were varied by varying light pulse intensity, were also accounted for (Figure 3G). All model parameters were statistically constrained by the data; 27 out of 29 parameters were fully identifiable from the data and the remaining two had upper 95% confidence bounds (Figure S6; Table S2). These findings imply that the model can be used to make quantitative predictions.

Transcription Rate Overshoots for Both *frq* and *vvd*

The double-light-pulse experiment (Cesbron et al., 2015) directly showed a refractory period for *frq* (cf. Figure 3A, lower panel) but not for *vvd*. The model selection suggests that *vvd* has nevertheless a refractory state but promoter activation is so inefficient that the first light pulse (low light intensity) leaves many promoters available for activation by the second high light pulse (see also below). However, irrespective of the efficiency of gene activation, the presence of a refractory gene state implies, on the population level, an initial overshoot in transcription rate. By contrast, without promoter refractoriness transcript levels should reach their respective steady state through a monotonic increase (cf. Figure 2D).

To test this prediction experimentally, we applied a constant light stimulus, enabling us to observe both the initial transient response of gene expression and the eventual steady state. The experimental data agreed closely with the respective model simulations (Figure 4A). Both *frq* and *vvd* mRNA levels overshot, whereas the WCC occupancy of the LREs of the genes was steady (Figures 4B and S7A). Moreover, the model predicts that *frq* shows a transcriptional overshoot already at lower light intensities than *vvd* (Figure 4A). To test this, we applied constant light stimuli of lower intensities, and measured the kinetics of luciferase induction from both *frq* and *vvd* gene promoters. To increase the sensitivity and temporal resolution of the measurements we used a PEST-destabilized luciferase reporter (Cesbron et al., 2013, 2015). As RT-PCR for mRNA was not quantitatively reliable at low induction levels we inferred the underlying time courses of mRNA computationally. Even if we made the conservative assumption of monotonically increasing signals of PEST-destabilized luciferase (thus strongly curtailing the impact of measurement noise on the inference of the mRNA kinetics), the data clearly implied overshooting mRNA levels for both genes and, moreover, showed the predicted higher excitability of *frq* (Figures 4C and S7B). Taken together, these data show that a transcriptional overshoot is an intrinsic property of the *frq* and *vvd* genes in response to a constant activating WCC signal, as predicted by the refractory-cycling model.

Differential Dose Responses of *frq* and *vvd* Are due to Different Activation Rates

To understand the mechanistic basis of the different responses of *frq and vvd* genes to WCC, we examined the model parameters inferred from the data (cf. Figure 3). The key parameters determining the dose response (Equation 2; Box 1) are the affinity for the transcriptional activator (measured by K_D), the initiation rate from the active promoter (f) and the lifetimes of the gene states (τ_I, τ_A and τ_R). The inferred average gene state lifetimes are between 36 and 65 min for the refractory state and between 10 and 20 min for the active state. The average lifetimes of the inactive state at maximal TF occupancy are inferred to be short, several seconds for *frq* and 1–3 min for *vvd* (for a summary of all parameter estimates see Table S2).

The model predicts that only two of these parameters, the transcription initiation rate and the lifetime of the inactive gene state, differ significantly between *frq and vvd* (Figure 5A; note that τ_I depends on WCC concentration and the diagram shows that the minimal values approached at high WCC levels). To test the prediction on different transcription rates, we quantified the gene occupancy by initiating RNA polymerase, which is marked by C-terminal phosphorylation at serine 5. Neither *frq* nor *vvd* show a peak of ''paused'' polymerase at their respective promoters, but rather have broad distributions of serine-5-phosphorylated polymerase in the promoter-proximal parts of the genes (Cesbron et al., 2015). Provided that the polymerase progression rates are similar for both genes, this polymerase occupancy can be considered as a proxy for initiation rate. The ~10-fold higher polymerase occupancy of the *vvd* promoter is consistent with the model prediction that the initiation rate from this promoter is about one order of magnitude larger than the *frq* initiation rate (Figure 5B).

The second differential parameter, the lifetime of the inactive gene state, yields very different dose responses of the two genes to WCC according to our theory (Figure 5C), which is indeed seen experimentally (Figure 5D). In particular, for the *frq* gene, we find that transcription rate saturated before WCC binding (Figure 5E). Hence, a remarkable prediction from the viewpoint of the classical theory of gene regulation is that the different dose responses of *frq* and *vvd* genes arise solely from different activation rates, whereas the WCC affinities of the two genes' LREs are predicted to be statistically indistinguishable (cf. Figure 5A).

(B) A total of 484 possible models of WCC action fitted to time-resolved data for *frq* and *vvd*, and ranked by the Akaike information criterion (AIC).
(C) The best four models for *frq* and *vvd* selected by AIC.
(D–G) Data versus best fit of Model 3 for: WCC binding (D), RNA dynamics (E), luciferase reporter varying double-light-pulse interval (F), and light pulse intensity (G) (LP, light pulse). The colors in (G) represent different intensities of light pulses used for gene induction. The shaded areas around the curves in (D–G) give the estimated errors of the data from the error model. See also Figures S5 and S6.

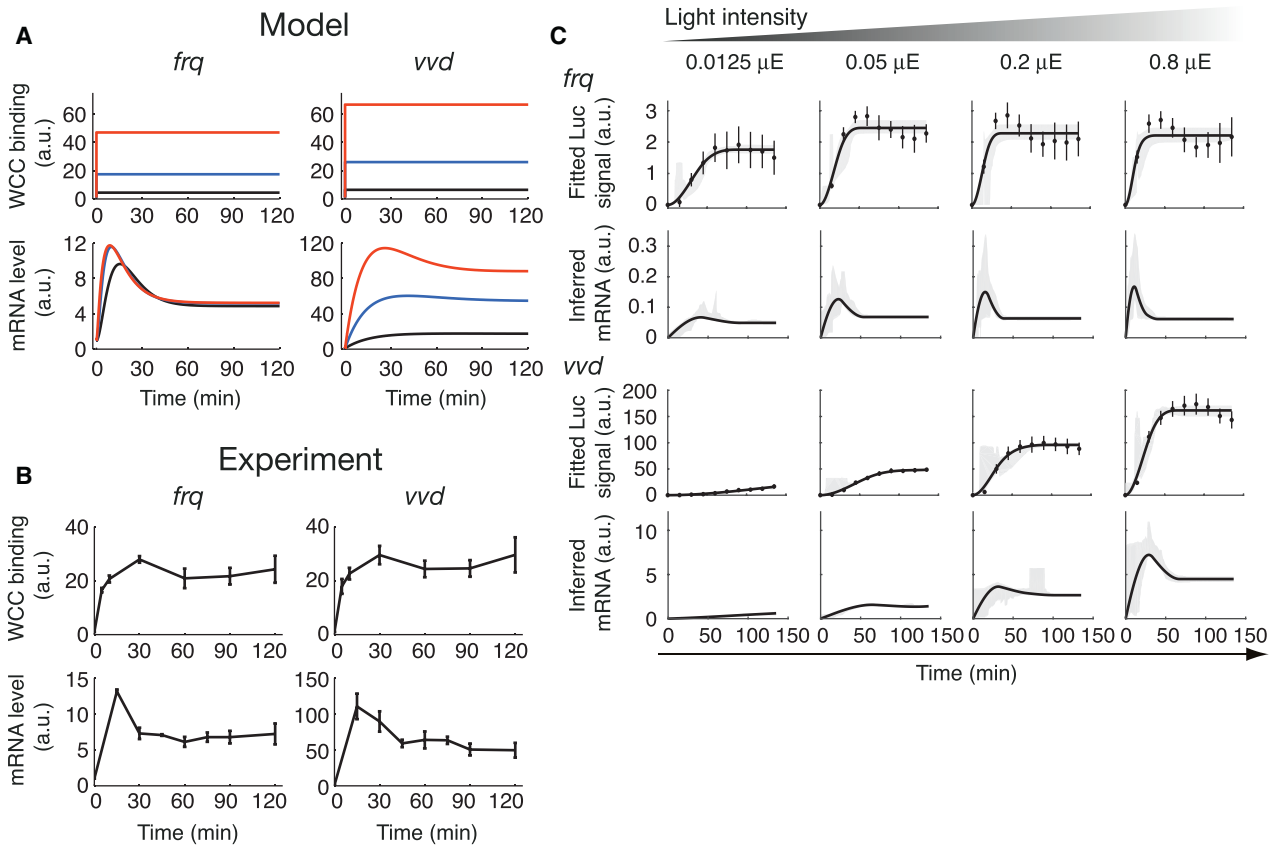

Figure 4. Transcriptional Overshoot of WCC Target Genes *frq* and *vvd*

(A) Simulation of mRNA dynamics of *frq* and *vvd* (lower panel) under constant WCC levels (upper panel), using the parameter values from the best fit.

(B) Experimental data of WCC binding (upper panel, chromatin immunoprecipitation-PCR) and mRNA dynamics of *frq* and *vvd* (lower panel, RT-PCR) under constant high light intensity (n = 3).

(C) Inference of mRNA kinetics from luciferase reporter kinetics under constant low light intensities (n = 4). The first row shows the fitting results for *frq* by monotonic cubic splines, and the second row is the inferred mRNA dynamics. The third and fourth rows show the same quantities for *vvd*. Shaded areas depict 95% confidence intervals determined by non-parametric bootstrap. Data in (B) and (C) are presented as mean ± SEM. See also Figure S7.

Indeed, the *frq* and *vvd* LREs share a common sequence grammar, both containing tandem GATC motifs for WCC binding, but differing somewhat in the number and spacing of the motifs (Sancar et al., 2015). Previous work has shown comparable WCC binding to the two LREs after light activation (Cesbron et al., 2015). To examine whether the small differences in LRE sequence cause differential gene regulation or, as indicated by the model, have no impact on the WCC dose response, we engineered a *vvd* construct replacing the original *vvd* LRE by the *frq* LRE (Table S3–S5). If the LRE sequence determined the sensitive WCC dose response of the *frq* gene (Figure 5F), then this swap should render the *vvd* gene sensitive to lower light intensities. However, LRE swapping did not alter the *vvd* dose response at all (Figure 5G). This absence of a specific LRE effect is consistent with the model prediction that the differential dose responses of *frq* and *vvd* are due to distinct lifetimes of the inactive gene state.

Enhancer-Promoter Distance and Core Promoter Encode Differential Gene Activation

The gene activation rate ($1/\tau_I$) is inversely proportional to the lifetime of the inactive gene state and depends on the level of active WCC inducing activation. A striking difference between *frq* and *vvd* is the placement of the respective LRE, proximal to the *frq* promoter (145 bp to transcription start site [TSS]; Figure 5F) and distal to the *vvd* promoter (1,632 bp to the TSS; Figure 5G). Indeed, the contact frequency of two sites on the chromatin fiber drops dramatically over this genomic distance (Ringrose et al., 1999). Therefore, we hypothesized that, at a given WCC occupancy of an LRE, the genomic distance between the LRE and the promoter controls the activation rate of the gene. To make testable predictions, we extended the mathematical model by decomposing promoter activation into a reversible chromatin looping step that brings LRE-bound WCC and the promoter into proximity and a subsequent transition from the inactive to the active gene state (Figure 6A; STAR Methods, Mathematical Modeling). Then the overall rate of gene activation becomes approximately:

$$\text{Activation rate} = \frac{1}{\tau_I(L)} \simeq \frac{1}{\tau_O} \frac{\tau_{\text{looped}}}{\tau_{\text{unlooped}}} = \frac{c j_M(L)}{\tau_O}, \qquad \text{(Equation 3)}$$

where τ_{unlooped} and τ_{looped}, respectively, are the average lifetimes of the unlooped state (no contact between LRE and TSS) and the

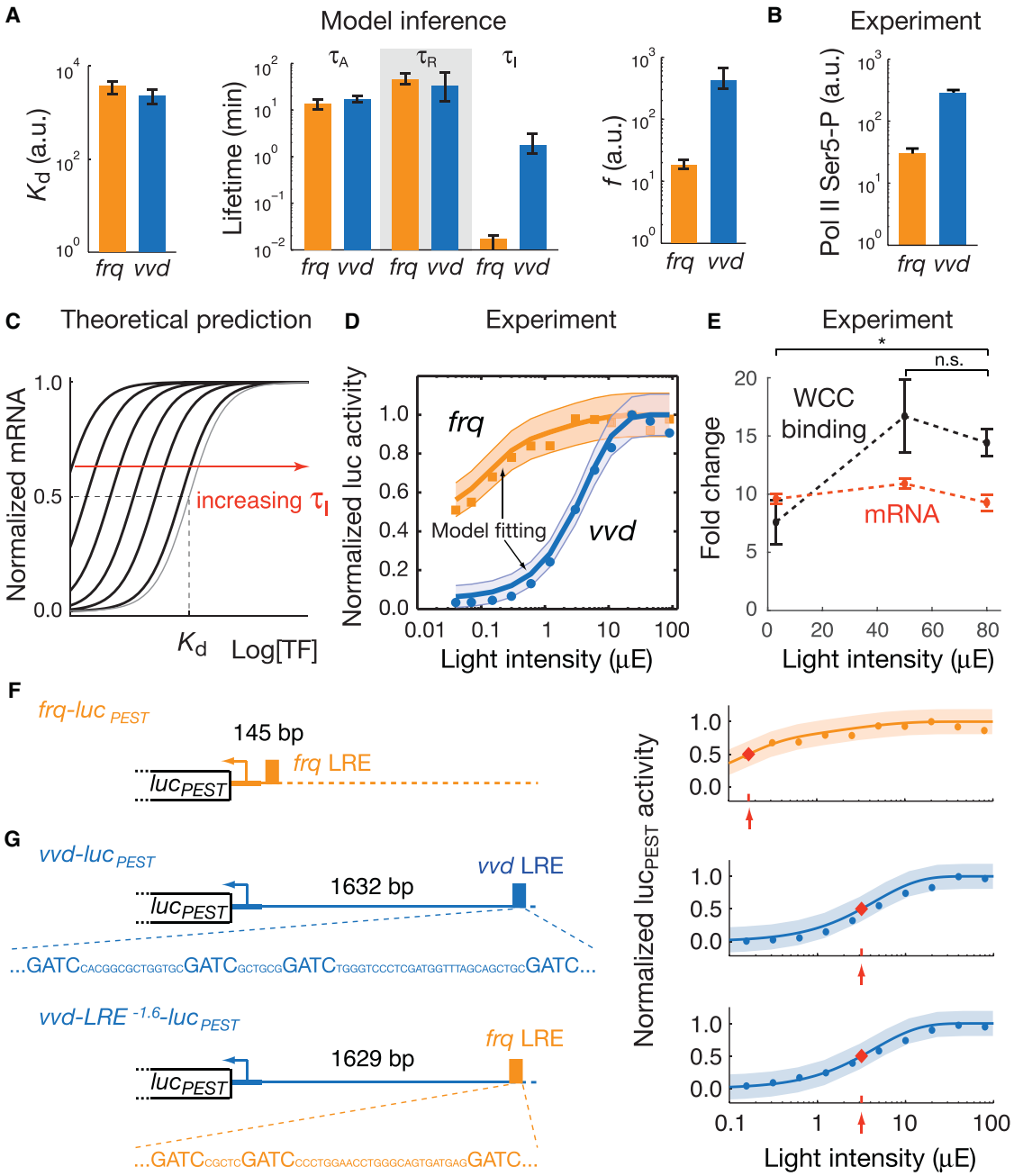

Figure 5. Identification of Key Parameters for Differential Gene Regulation of WCC Target Genes

(A) Comparison of inferred key parameters between *frq* and *vvd*, with 95% confidence bounds.

(B) Experimental quantification of RNA polymerase C-terminal tail phosphorylation at Ser5 within *frq* and *vvd* (marker for transcription initiation). Error bars indicate SEM.

(C) Theoretical prediction of the mRNA dose-response (normalized by maximum level) by varying τ_I.

(D) Differential responses (quantified by normalized luciferase signals) of *frq* (orange) and *vvd* (blue) to light-activated WCC, which were obtained from Figure 3G. Dots and squares, experimental data; solid curves, best fit of the model; shaded areas, estimated errors.

(E) Fold change in WCC occupancy (black) and mRNA level (red) for *frq* with different light pulse intensities (± SEM; n = 3). n.s., not significant; *p < 0.05, two-sample t test. Pairwise tests of all mRNA levels (n = 3) show no significant difference.

(F and G) Prediction and validation of LRE-swapping. Left panels, construct design (with GATC motifs in LREs); right panels, theoretical prediction (solid lines and shaded 95% confidence bands) and experimental data (dots). Red diamonds show the predicted operating points. Model 3 was used throughout (see Figure 3C). See also Table S2.

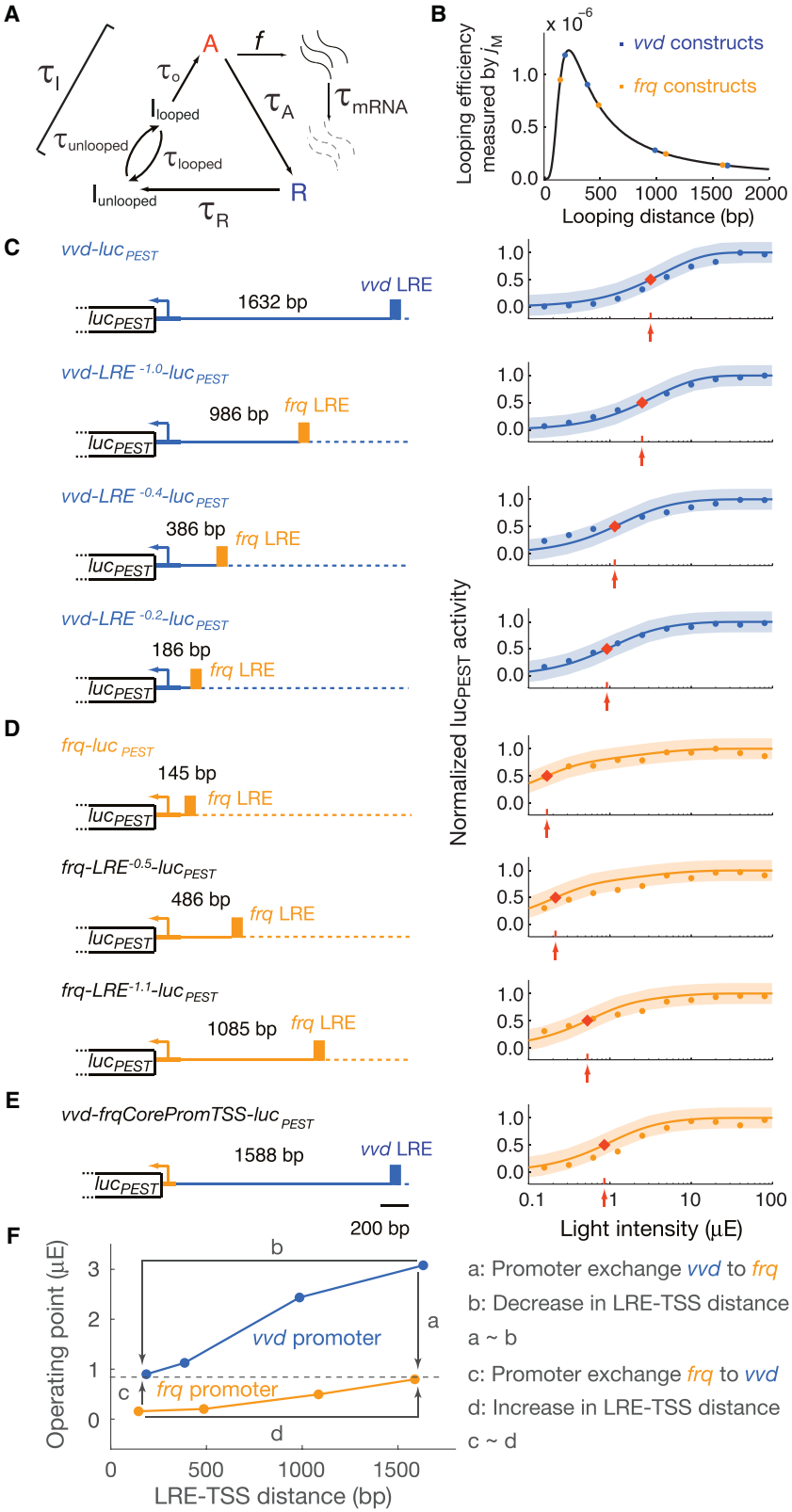

Figure 6. Differential Gene Regulation by Promoter-LRE Distance

(A) Extended model incorporating switching between an unlooped state (with lifetime $\tau_{unlooped}$) and a looped state (with lifetime τ_{looped}), coupled with an irreversible transition from looped to active promoter state (with characteristic time τ_O).

(B) Chromatin looping efficiency j_M as a function of the genomic distance between two sites on the chromatin. Blue and orange dots mark the *vvd* and *frq* constructs used in (C–E), respectively.

(C–E) Left panels show *vvd* and *frq* constructs with various LRE-TSS distances measured from the center of LRE to TSS. The right panels show the corresponding model prediction (solid lines, with shaded 95% confidence bands; red diamonds, predicted operating points) and experimental data (dots) (n = 3 for each construct and light intensity).

(F) LRE-TSS distance and core promoter jointly determine the operating points of the *frq* and *vvd* dose responses to WCC (in units of light pulse intensity). Dots represent the operating points in the model (which are characteristic of the experimentally observed ones), see (C–E); labeled arrows correspond to two kinds of experimental manipulation: promoter exchanges (A and C) and changes in LRE-TSS distance by ~1.4 kb (B and D). For a given gene, the two manipulations have similar quantitative effects.

looped state (WCC-occupied LRE and TSS in contact); j_M denotes the effective concentration of the LRE with respect to the TSS according to standard polymer theory and c is a constant (Chen et al., 2014). The new parameter τ_O is the opening time for the promoter following enhancer-promoter looping; it may be gene specific. Thus Equation 3 connects the activation rate to the chromatin looping distance via $j_M(L)$ (Figure 6B). Of note, this extension of the model does not introduce new free parameters, as $j_M(L)$ has been measured (Ringrose et al., 1999), and then the promoter opening time τ_O is fixed by the already inferred values of τ_I for *frq* and *vvd*. Hence, the activation rate for a gene following TF binding is determined by a promoter-specific component, the opening time (τ_O) and the genomic distance between enhancer and promoter (L).

To test the hypothesis that gene activation rate controls its TF sensitivity, we first changed the gene activation rate according to Equation 3 in the model by varying the LRE-TSS distance (Figure 6B). The theoretically predicted dose-response curves for *vvd* and *frq* showed an increase in activator sensitivity with decreasing LRE-TSS distance (Figure 6C, solid lines and shaded areas). We generated luciferase constructs driven by the *vvd* core promoter and the *frq* LRE inserted at different distances from the TSS. *vvd* expression is rendered increasingly sensitive to WCC by bringing the LRE closer to the promoter (Figure 6C, blue dots), which agrees quantitatively with the predictions of the mathematical model. To test the effect of the reverse manipulation (moving the LRE away from the promoter) we drove luciferase expression from the *frq* core promoter, with the *frq* LRE being gradually dislodged from its wild-type promoter-proximal location. These data again agreed with the model prediction in showing that the gene gradually loses sensitivity to the TF (Figure 6D). Thus, the genomic distance between promoter and *cis*-regulatory element (LRE) determines the gene's sensitivity to its activator. Finally, apart from the distance, Equation 3 also contains the gene specific parameter τ_O. We introduced the *frq* core promoter into the *vvd* gene and found that the experimental data matched the theoretical predictions obtained with model containing the τ_O for *frq* and the *vvd* LRE-promoter distance (Figure 6E). These data show that the gene-specific parameter τ_O is a function of the core promoter.

Collectively, these findings provide strong support for the model prediction that gene activation rate, and not WCC-LRE affinity, determines the differential regulation of the *vvd* and *frq* genes. The gene activation rate is set by the genomic distance between promoter and *cis*-regulatory element and by a promoter-specific component. Quantitatively, the effect of putting the more slowly activated *vvd* promoter in place of the *frq* promoter is approximately the same as moving the *frq* LRE 1.4 kb away from its native site, and vice versa for the *vvd-frq* promoter swap (Figure 6F). Thus, for the two genes studied here, the effects of core promoter and genomic distance on activation rate balance.

DISCUSSION

Transcription belongs to the most complex enzymatic processes in the cell, yet a compellingly simple "effective" model that relates transcription rate to equilibrium distributions of TF binding, has been widely used to quantitate its regulation. Predictions with this model on a large-scale basis, however, are far from perfect (Segal et al., 2008). As experimental tools are becoming more sophisticated, complex relationships between TF binding sequences, TF occupancy, and transcript abundance are being found, thus suggesting that sequence-controlled TF occupancy may not directly convert into transcription rate (Spitz and Furlong, 2012; Bentovim et al., 2017). For example, in two *Drosophila* species, Khoueiry et al. (2017) found conserved combinatorial TF occupancy despite sequence divergence, and conserved enhancer function despite diverged occupancy. Indeed, regulated accessibility of chromatin for TFs and the general transcription machinery has emerged as a prime determinant of transcription rate in eukaryotes. While the chromatin state may be locally controlled by sequence-specific TFs, the downstream reactions, such as nucleosome remodeling and posttranslational histone modifications, are highly dynamic non-equilibrium processes that consume metabolic energy (Coulon et al., 2013; Voss and Hager, 2014) and thus may "process" the information contained in TF binding in unexpected ways (Ahsendorf et al., 2014; Estrada et al., 2016; Scholes et al., 2017). Here we proposed a simple yet generic model of non-equilibrium gene regulation and demonstrated its utility in gaining insight from experimental data.

We based our theory on observable properties of transcriptional bursting dynamics, namely the existence of long-lived active, inactive, and refractory gene states. Interestingly, the lifetimes of these states inferred here for *Neurospora* genes (between 30 min and 1 hr combined for refractory and inactive states, and between 10 and 20 min for the active state) are rather similar to the values for mammalian genes derived from live-cell imaging (one to several hours for the refractory state and of the order of 10 min for the active state; Harper et al., 2011; Suter et al., 2011).

While our derivation of gene-regulatory functions does not rely on detailed knowledge about the molecular nature of the states, the confrontation of the models with experimental data provided concrete leads to molecular mechanisms. Systematic model selection identified the key role of the TF studied, the GATA-factor WCC, as enhancing the transition from the inactive to the active gene state. Indeed, WCC, as many other TFs, recruits nucleosome remodelers and causes nucleosome eviction (Sancar et al., 2015). Thus, our findings are in line with studies showing that TF-induced nucleosome remodeling is rate limiting for transcriptional activation (Boeger et al., 2008; Kim and O'Shea, 2008). Interestingly, model selection rules out a direct effect of WCC on transcription initiation rate, indicating that other factors quantitatively control RNA polymerase recruitment and/or transcription initiation after the gene transits into an active state. Our findings further imply that TFs such as WCC may only need to interact transiently with their target genes to activate them. This transient effect has indeed been observed for the glucocorticoid receptor in mammalian cells (Voss et al., 2011), where extremely short DNA binding events (seconds) have a lasting effect on chromatin accessibility for downstream regulators of transcription. Further supporting this idea, we observed here that activation of *frq* transcription by WCC reached its maximum long before WCC binding to the respective enhancer element (LRE) became saturating. Moreover, a recent theoretical study has shown how the transient action of multiple TFs on the

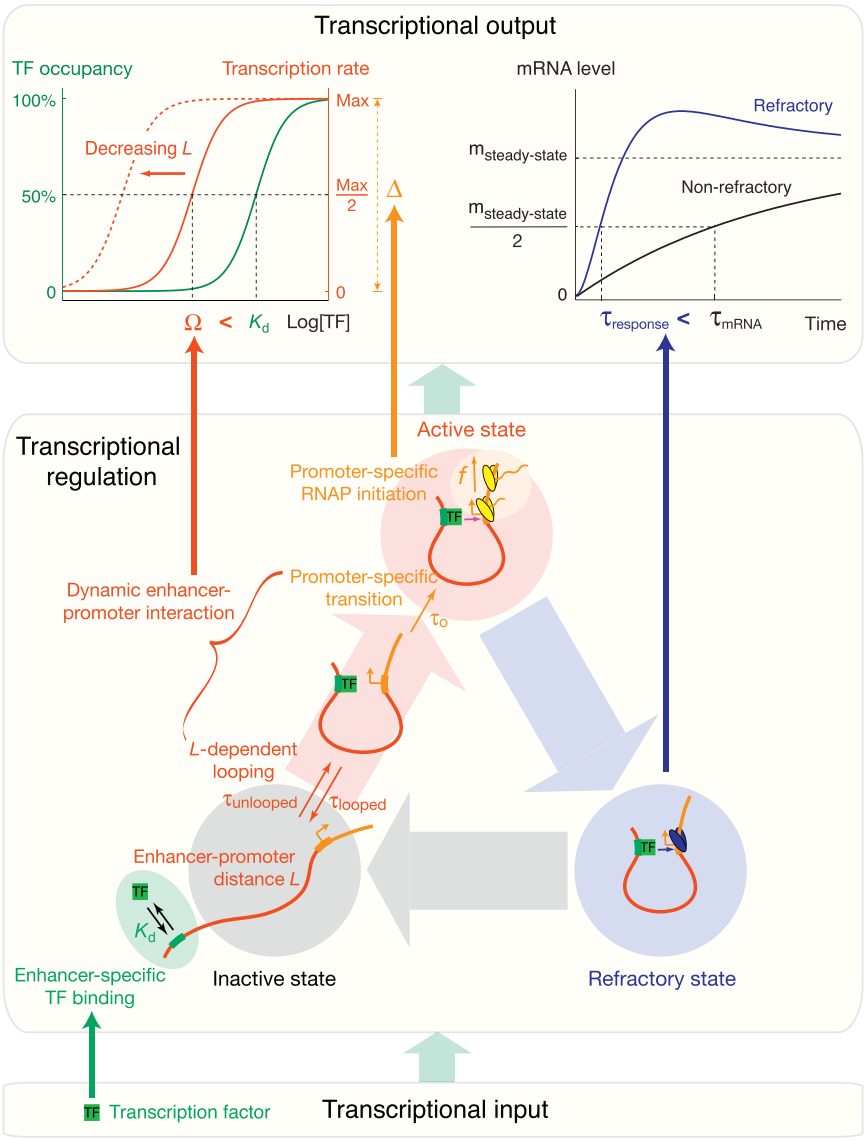

Figure 7. Gene Regulation within a Non-equilibrium Framework

TF binding (depending on K_D and [TF]) signals gene activation mediated, e.g., by chromatin remodeling. The rate of gene activation, which is governed by enhancer-promoter distance (L) and a promoter-specific rate component τ_O, determines how sensitive a gene responds to the TF. Thus transient TF occupancy may cause full gene activation. The presence of a refractory state enables rapid responses to stimuli.

transcription cycle can cause combinatorial regulation of transcription rate without physical TF interactions, which has been termed kinetic control (Scholes et al., 2017).

Following this lead by the theory allowed us to identify a specific non-equilibrium mechanism that governs differential expression of WCC target genes. Judged from the viewpoint of (equilibrium) TF occupancy, the *vvd* and *frq* LREs are very similar, containing, respectively, four and three GATC binding motifs. In agreement with these sequence properties, WCC occupancies are similar at the two LREs, with *vvd* having somewhat higher occupancy (Cesbron et al., 2015). However, transcription of the *frq* gene is much more sensitive to WCC concentration.

Model-based inference from the experimental data shows that the differential sensitivities of *frq* and *vvd* transcription to WCC are controlled by a kinetic parameter: the gene activation rate. Based on the known enhancer configurations for two key WCC target genes, *frq* and *vvd*, we reasoned that the rate of dynamic enhancer-promoter interactions, governed by genomic distance, determines the gene activation rate (Figure 7). The quantitative comparison of theory with experiment also identified a promoter-specific component in setting the gene's activation rate, which had a similar quantitative effect on gene regulation as genomic distance. Remarkably, tuning these two regulators of the gene activation rate allows differential gene activation without differences in TF binding affinity or occupancy.

While the model was parameterized here for light-controlled transcription in *Neurospora*, we expect it to be more broadly applicable. A recent elegant study in *Drosophila* embryos supports the notion that enhancer-promoter associations are dynamic by showing that two genes can be transcribed at the same time under the control of a shared enhancer, which, incidentally, controls transcription burst frequency of the genes (Fukaya et al., 2016). In mammalian cells, forced enhancer-promoter looping also causes an increase in burst frequency (Bartman et al., 2016). Promoter-enhancer distance may control gene activation rate also by mechanisms other than direct looping. In particular, chromatin states may propagate by autocatalytic mechanisms (Angel et al., 2011; Berry et al., 2015), which, however, may also involve chromatin looping as a parameter (Müller-Ott et al., 2014). We would like to emphasize, however, that the key feature of our model is that burst frequency modulation by a TF allows highly sensitive gene regulation. Genomic distance is only one of several molecular parameters that could impact on frequency modulation.

Furthermore, coupling burst frequency modulation with inherent promoter refractoriness allows the transcript to overshoot its steady state when the upstream TF becomes active. This hallmark of transcriptional refractoriness has an implication for the precision of a gene's response to stimuli, on both cell-population and single-cell levels. In a single cell, the first transcription burst induced by a stimulus can already yield the full transcriptional response also seen after a sustained stimulus,

because after a brief period of activity, the gene enters a long refractory period, during which it remains insensitive to stimulation. Therefore, a refractory gene can give a unique and precise answer to a stimulus regardless of the time duration it is applied. In *Neurospora*, WCC and VVD proteins are light sensors that govern the entrainment of the circadian clock to the day-night cycle and its adaptation to continuous light, respectively (Malzahn et al., 2010; Gin et al., 2013). Precise responses to light stimuli that fluctuate with weather and growth environment of the fungus might be critical here for robust function. By contrast, transcripts of a refractory gene with slow activation rate or a non-refractory gene (as in the telegraph model) will build up incrementally in single cells before the full response is reached, and thus the answer will be strongly controlled by signal duration in this case. Both response modes, full response on first trigger versus buildup of response with stimulus length, may be appropriate in different functional contexts. With the increasing body of evidence showing that dynamic input stimuli differentially regulate gene expression and cell fate (Purvis and Lahav, 2013), the dissection of the transcription cycles of target genes should provide insight into the mechanisms underlying specificity.

The basic line of reasoning in this study is that ''microscopic'' properties of the transcription cycle, such as the lifetimes of inactive, active, and refractory gene states, have ''macroscopic'' consequences on gene regulation that determine the regulatory logic at the level of the cell population. However, our theoretical framework can equally be applied to study variability and robustness of gene expression at the single-cell level.

STAR★METHODS

Detailed methods are provided in the online version of this paper and include the following:

- KEY RESOURCES TABLE
- CONTACT FOR REAGENT AND RESOURCE SHARING
- EXPERIMENTAL MODEL AND SUBJECT DETAILS
  - Culture Conditions
- METHOD DETAILS
  - Plasmid Construction and *Neurospora* Transformation
  - RNA Analysis
  - *In Vivo* Luciferase Measurements
  - Antibodies
  - Chromatin Immunoprecipitation (ChIP)
  - RNA and ChIP Sequencing
  - Sequencing Data Analysis
  - Mathematical Modeling
- QUANTIFICATION AND STATISTICAL ANALYSIS

SUPPLEMENTAL INFORMATION

Supplemental Information includes seven figures and five tables and can be found with this article online at https://doi.org/10.1016/j.cels.2018.01.012.

ACKNOWLEDGMENTS

We thank the members of the Höfer group, especially Xi Wang, and the Brunner group, as well as Naama Barkai for stimulating discussions. This work was supported by grants from the DFG (SFB1036 to M.B.), the European Commission (FP7 Sysmed-IBD to T.H.), and DKFZ core funding. M.B. and T.H. are members of CellNetworks.

AUTHOR CONTRIBUTIONS

T.H. and M.B. supervised the study. C.L. performed the modeling. F.C. and M.O. carried out the experiments. C.L., F.C., M.B., and T.H. analyzed the data. T.H., C.L., and M.B. conceived the study and wrote the paper.

DECLARATION OF INTERESTS

The authors declare no competing interests.

Received: August 1, 2017
Revised: November 16, 2017
Accepted: January 11, 2018
Published: February 14, 2018

REFERENCES

Ahsendorf, T., Wong, F., Eils, R., and Gunawardena, J. (2014). A framework for modelling gene regulation which accommodates non-equilibrium mechanisms. BMC Biol. *12*, 102.

Akaike, H. (1974). A new look at the statistical model identification. IEEE Trans. Autom. Control *19*, 716–723.

Alberts, B., Johnson, A., Lewis, J., Morgan, D., Raff, M., Roberts, K., and Walter, P. (2015). Molecular Biology of the Cell (Garland Science).

Angel, A., Song, J., Dean, C., and Howard, M. (2011). A Polycomb-based switch underlying quantitative epigenetic memory. Nature *476*, 105–108.

Bartman, C.R., Hsu, S.C., Hsiung, C.C.-S., Raj, A., and Blobel, G.A. (2016). Enhancer regulation of transcriptional bursting parameters revealed by forced chromatin looping. Mol. Cell *62*, 237–247.

Battich, N., Stoeger, T., and Pelkmans, L. (2015). Control of transcript variability in single mammalian cells. Cell *163*, 1596–1610.

Ben-Ari, Y., Brody, Y., Kinor, N., Mor, A., Tsukamoto, T., Spector, D.L., Singer, R.H., and Shav-Tal, Y. (2010). The life of an mRNA in space and time. J. Cell Sci. *123*, 1761–1774.

Bentovim, L., Harden, T.T., and DePace, A.H. (2017). Transcriptional precision and accuracy in development: from measurements to models and mechanisms. Dev. Camb. Engl. *144*, 3855–3866.

Berry, S., Hartley, M., Olsson, T.S.G., Dean, C., and Howard, M. (2015). Local chromatin environment of a Polycomb target gene instructs its own epigenetic inheritance. Elife *4*, e07205.

Bintu, L., Buchler, N.E., Garcia, H.G., Gerland, U., Hwa, T., Kondev, J., and Phillips, R. (2005). Transcriptional regulation by the numbers: models. Curr. Opin. Genet. Dev. *15*, 116–124.

Boeger, H., Griesenbeck, J., and Kornberg, R.D. (2008). Nucleosome retention and the stochastic nature of promoter chromatin remodeling for transcription. Cell *133*, 716–726.

Cesbron, F., Brunner, M., and Diernfellner, A.C.R. (2013). Light-dependent and circadian transcription dynamics in vivo recorded with a destabilized luciferase reporter in *Neurospora*. PLoS One *8*, e83660.

Cesbron, F., Oehler, M., Ha, N., Sancar, G., and Brunner, M. (2015). Transcriptional refractoriness is dependent on core promoter architecture. Nat. Commun. *6*, 6753.

Chen, Y.-J., Johnson, S., Mulligan, P., Spakowitz, A.J., and Phillips, R. (2014). Modulation of DNA loop lifetimes by the free energy of loop formation. Proc. Natl. Acad. Sci. USA *111*, 17396–17401.

Coulon, A., Chow, C.C., Singer, R.H., and Larson, D.R. (2013). Eukaryotic transcriptional dynamics: from single molecules to cell populations. Nat. Rev. Genet. *14*, 572–584.

Dar, R.D., Razooky, B.S., Singh, A., Trimeloni, T.V., McCollum, J.M., Cox, C.D., Simpson, M.L., and Weinberger, L.S. (2012). Transcriptional burst frequency and burst size are equally modulated across the human genome. Proc. Natl. Acad. Sci. USA *109*, 17454–17459.

Estrada, J., Wong, F., DePace, A., and Gunawardena, J. (2016). Information integration and energy expenditure in gene regulation. Cell *166*, 234–244.

Friedman, N., Cai, L., and Xie, X.S. (2006). Linking stochastic dynamics to population distribution: an analytical framework of gene expression. Phys. Rev. Lett. *97*, 168302.

Fukaya, T., Lim, B., and Levine, M. (2016). Enhancer control of transcriptional bursting. Cell *166*, 358–368.

Gin, E., Diernfellner, A.C.R., Brunner, M., and Höfer, T. (2013). The *Neurospora* photoreceptor VIVID exerts negative and positive control on light sensing to achieve adaptation. Mol. Syst. Biol. *9*, 667.

Giorgetti, L., Siggers, T., Tiana, G., Caprara, G., Notarbartolo, S., Corona, T., Pasparakis, M., Milani, P., Bulyk, M.L., and Natoli, G. (2010). Noncooperative interactions between transcription factors and clustered DNA binding sites enable graded transcriptional responses to environmental inputs. Mol. Cell *37*, 418–428.

Harper, C.V., Finkenstädt, B., Woodcock, D.J., Friedrichsen, S., Semprini, S., Ashall, L., Spiller, D.G., Mullins, J.J., Rand, D.A., Davis, J.R.E., et al. (2011). Dynamic analysis of stochastic transcription cycles. PLoS Biol. *9*, e1000607.

Hornung, G., Bar-Ziv, R., Rosin, D., Tokuriki, N., Tawfik, D.S., Oren, M., and Barkai, N. (2012). Noise-mean relationship in mutated promoters. Genome Res. *22*, 2409–2417.

Ietswaart, R., Rosa, S., Wu, Z., Dean, C., and Howard, M. (2017). Cell-size-dependent transcription of FLC and its antisense long non-coding RNA COOLAIR explain cell-to-cell expression variation. Cell Syst. *4*, 622–635.e9.

Khoueiry, P., Girardot, C., Ciglar, L., Peng, P.C., Gustafson, E.H., Sinha, S., and Furlong, E.E. (2017). Uncoupling evolutionary changes in DNA sequence, transcription factor occupancy and enhancer activity. Elife *6*, https://doi.org/10.7554/eLife.28440.

Kim, H.D., and O'Shea, E.K. (2008). A quantitative model of transcription factor-activated gene expression. Nat. Struct. Mol. Biol. *15*, 1192–1198.

Kreutz, C., Raue, A., and Timmer, J. (2012). Likelihood based observability analysis and confidence intervals for predictions of dynamic models. BMC Syst. Biol. *6*, 1–9.

Larson, D.R., Fritzsch, C., Sun, L., Meng, X., Lawrence, D.S., and Singer, R.H. (2013). Direct observation of frequency modulated transcription in single cells using light activation. Elife *2*, https://doi.org/10.7554/eLife.00750.

Lefstin, J.A., and Yamamoto, K.R. (1998). Allosteric effects of DNA on transcriptional regulators. Nature *392*, 885–888.

Luijsterburg, M.S., von Bornstaedt, G., Gourdin, A.M., Politi, A.Z., Moné, M.J., Warmerdam, D.O., Goedhart, J., Vermeulen, W., van Driel, R., and Höfer, T. (2010). Stochastic and reversible assembly of a multiprotein DNA repair complex ensures accurate target site recognition and efficient repair. J. Cell Biol. *189*, 445–463.

Malzahn, E., Ciprianidis, S., Káldi, K., Schafmeier, T., and Brunner, M. (2010). Photoadaptation in *Neurospora* by competitive interaction of activating and inhibitory LOV domains. Cell *142*, 762–772.

Molina, N., Suter, D.M., Cannavo, R., Zoller, B., Gotic, I., and Naef, F. (2013). Stimulus-induced modulation of transcriptional bursting in a single mammalian gene. Proc. Natl. Acad. Sci. USA *110*, 20563–20568.

Morisaki, T., Müller, W.G., Golob, N., Mazza, D., and McNally, J.G. (2014). Single-molecule analysis of transcription factor binding at transcription sites in live cells. Nat. Commun. *5*, 4456.

Müller-Ott, K., Erdel, F., Matveeva, A., Mallm, J.P., Rademacher, A., Hahn, M., Bauer, C., Zhang, Q., Kaltofen, S., Schotta, G., et al. (2014). Specificity, propagation, and memory of pericentric heterochromatin. Mol. Syst. Biol. *10*, 746.

Neuert, G., Munsky, B., Tan, R.Z., Teytelman, L., Khammash, M., and van Oudenaarden, A. (2013). Systematic identification of signal-activated stochastic gene regulation. Science *339*, 584–587.

Nicolas, D., Phillips, N.E., and Naef, F. (2017). What shapes eukaryotic transcriptional bursting? Mol. Biosyst. *13*, 1280–1290.

Peccoud, J., and Ycart, B. (1995). Markovian modeling of gene-product synthesis. Theor. Popul. Biol. *48*, 222–234.

Ptashne, M., and Gann, A. (2002). Genes and Signals (Cold Spring Harbor Laboratory Press).

Purvis, J.E., and Lahav, G. (2013). Encoding and decoding cellular information through signaling dynamics. Cell *152*, 945–956.

Raj, A., and van Oudenaarden, A. (2008). Nature, nurture, or chance: stochastic gene expression and its consequences. Cell *135*, 216–226.

Raue, A., Steiert, B., Schelker, M., Kreutz, C., Maiwald, T., Hass, H., Vanlier, J., Tönsing, C., Adlung, L., Engesser, R., et al. (2015). Data2Dynamics: a modeling environment tailored to parameter estimation in dynamical systems. Bioinformatics *31*, 3558–3560.

Ringrose, L., Chabanis, S., Angrand, P.O., Woodroofe, C., and Stewart, A.F. (1999). Quantitative comparison of DNA looping in vitro and in vivo: chromatin increases effective DNA flexibility at short distances. EMBO J. *18*, 6630–6641.

Rosenfeld, N., Elowitz, M.B., and Alon, U. (2002). Negative autoregulation speeds the response times of transcription networks. J. Mol. Biol. *323*, 785–793.

Rosenfeld, N., Young, J.W., Alon, U., Swain, P.S., and Elowitz, M.B. (2005). Gene regulation at the single-cell level. Science *307*, 1962–1965.

Sancar, C., Ha, N., Yilmaz, R., Tesorero, R., Fisher, T., Brunner, M., and Sancar, G. (2015). Combinatorial control of light induced chromatin remodeling and gene activation in *Neurospora*. PLoS Genet. *11*, e1005105.

Sanchez, A., and Golding, I. (2013). Genetic determinants and cellular constraints in noisy gene expression. Science *342*, 1188–1193.

Savageau, M.A. (1974). Comparison of classical and autogenous systems of regulation in inducible operons. Nature *252*, 546–549.

Scholes, C., DePace, A.H., and Sánchez, Á. (2017). Combinatorial gene regulation through kinetic control of the transcription cycle. Cell Syst. *4*, 97–108.e9.

Schwanhausser, B., Busse, D., Li, N., Dittmar, G., Schuchhardt, J., Wolf, J., Chen, W., and Selbach, M. (2011). Global quantification of mammalian gene expression control. Nature *473*, 337–342.

Segal, E., Raveh-Sadka, T., Schroeder, M., Unnerstall, U., and Gaul, U. (2008). Predicting expression patterns from regulatory sequence in *Drosophila* segmentation. Nature *451*, 535–540.

Senecal, A., Munsky, B., Proux, F., Ly, N., Braye, F.E., Zimmer, C., Mueller, F., and Darzacq, X. (2014). Transcription factors modulate c-Fos transcriptional bursts. Cell Rep. *8*, 75–83.

Setty, Y., Mayo, A.E., Surette, M.G., and Alon, U. (2003). Detailed map of a *cis*-regulatory input function. Proc. Natl. Acad. Sci. USA *100*, 7702–7707.

Spitz, F., and Furlong, E.E.M. (2012). Transcription factors: from enhancer binding to developmental control. Nat. Rev. Genet. *13*, 613–626.

Suter, D.M., Molina, N., Gatfield, D., Schneider, K., Schibler, U., and Naef, F. (2011). Mammalian genes are transcribed with widely different bursting kinetics. Science *332*, 472–474.

Teif, V.B., Erdel, F., Beshnova, D.A., Vainshtein, Y., Mallm, J.-P., and Rippe, K. (2013). Taking into account nucleosomes for predicting gene expression. Methods *62*, 26–38.

Verbruggen, P., Heinemann, T., Manders, E., von Bornstaedt, G., van Driel, R., and Höfer, T. (2014). Robustness of DNA repair through collective rate control. PLoS Comput. Biol. *10*, e1003438.

Voss, T.C., and Hager, G.L. (2014). Dynamic regulation of transcriptional states by chromatin and transcription factors. Nat. Rev. Genet. *15*, 69–81.

Voss, T.C., Schiltz, R.L., Sung, M.-H., Yen, P.M., Stamatoyannopoulos, J.A., Biddie, S.C., Johnson, T.A., Miranda, T.B., John, S., and Hager, G.L. (2011). Dynamic exchange at regulatory elements during chromatin remodeling underlies assisted loading mechanism. Cell *146*, 544–554.

Zechner, C., Unger, M., Pelet, S., Peter, M., and Koeppl, H. (2014). Scalable inference of heterogeneous reaction kinetics from pooled single-cell recordings. Nat. Methods *11*, 197–202.

Zoller, B., Nicolas, D., Molina, N., and Naef, F. (2015). Structure of silent transcription intervals and noise characteristics of mammalian genes. Mol. Syst. Biol. *11*, 823.

STAR★METHODS

KEY RESOURCES TABLE

REAGENT or RESOURCE	SOURCE	IDENTIFIER
Antibodies		
Rabbit polyclonal anti-WC2	Cesbron et al., 2015	N/A
Chemicals, Peptides, and Recombinant Proteins		
peqGOLD TriFAST	PeqLab	Cat# 30-2010
Critical Commercial Assays		
QuantiTect reverse transcription kit	Qiagen	Cat#205310
StepOnePlus real-time PCR system	Applied Biosystems	Cat#4376600
TaqMan Gene Expression Master Mix	Applied Biosystems	Cat#4369016
TaqMan, and UPL probes	Roche	Cat#04869877001
Experimental Models: Organisms/Strains		
Neurospora crassa	Fungal Genetics Stock Center	FGSC #6103
Oligonucleotides		
Primers for *frq* and *vvd* hybrid luc_{PEST} constructs: see Table S4	This paper	N/A
Primers and probes for qRT-PCR and ChIP-qPCR: see Table S5	Cesbron et al., 2015	N/A
Recombinant DNA		
Plasmid: pFH62-frqΔup lucPEST	Cesbron et al., 2015	N/A
Plasmid: pFH62-vvd lucPEST	Cesbron et al., 2013	N/A
Software and Algorithms		
Data2Dynamics	Raue et al., 2015	http://www.data2dynamics.org

CONTACT FOR REAGENT AND RESOURCE SHARING

Further information and requests for resources and reagents should be directed to and will be fulfilled by the Lead Contact Thomas Höfer (t.hoefer@dkfz.de).

EXPERIMENTAL MODEL AND SUBJECT DETAILS

Culture Conditions

Standard growth medium contained 2 % glucose, 0.5 % L-arginine, 1× Vogel's medium. If not indicated otherwise, cells were grown 36 h in constant light (LL) and 24 h in constant darkness (DD) before the specific light treatment.

METHOD DETAILS

Plasmid Construction and *Neurospora* Transformation

A *pFH62-frqΔup* luc_{PEST} plasmid (Cesbron et al., 2015) was used as parental plasmid. The synthetic promoter contains a *SphI and a Asc1 site 107 bp* upstream and 153 bp downstream of the TSS (+1), respectively.

Different *frq* hybrid luc_{PEST} constructs (*frq-frqLRE*$^{-0.5}$ luc_{PEST} and *frq-frqLRE*$^{-1.1}$ luc_{PEST}) were created by inserting various lengths (657 bp and 1257 bp) of *frqΔLRE* fragment (Table S3) into the SphI and AscI sites of *frqΔup* luc_{PEST}.

Similarly different *vvd* hybrid luc_{PEST} constructs (*vvd-frqLRE*$^{-0.2}$ luc_{PEST}, *vvd-frqLRE*$^{-0.4}$ luc_{PEST} ,*vvd-frqLRE*$^{-1.0}$ luc_{PEST} and *vvd-frqLRE*$^{-1.6}$ luc_{PEST}) were created by inserting various lengths (457 bp, 657 bp, 1257 bp and 1900 pb) of *vvd* promoter fragment into the SphI and AscI sites of *frqΔup* luc_{PEST}.

Construction of the vector containing *vvd-frqCorePromTSS* luc_{PEST} was performed in two steps. A *pFH62-vvd* luc_{PEST} plasmid (Cesbron et al., 2013) was used as parental plasmid. A SphI site was introduced by site-directed mutagenesis upstream of the *vvd* transcriptional start site (-111). A 92 bp fragment containing *frq core promoter* was amplified by PCR and inserted in place of *vvd* transcriptional start site into the SphI and NotI sites.

Luc_{PEST} reporter genes were inserted into the his-3 locus of the indicated *bd* strains. Primers are listed in Table S4.

The sequences of *frq* and *vvd* LRE are, respectively: GGGACCGGACGACGGCTGGCCAATTAGACGGCCGTCGCAGAGGACCCT GAACTTTTC**GATC**CGCTC**GATC**CCCTGGAACCTGGGCAGTGATGAG**GATC**GGGGCGATTCCTGT GCGGTTTCAATTGTTCGTGC TGGCGCGTGGGTCCCGTTCTTGGTTC**GATC**CACGGCGCTGGTGC**GATC**GCTGCG**GATC**TGGGTCCCTCGATGGTTTAGCAGCT GC**GATC**GGTCAGCATCGCTGTCCCCATTCTACACTGCCATCCAAAATC

The GATC motifs are highlighted.

RNA Analysis

RNA was prepared with peqGOLD TriFAST (PeqLab). The reverse transcription was done with the QuantiTect reverse transcription kit (Qiagen) following the manufacturer's instructions. Transcript levels were analysed by quantitative real-time PCR in 96-well plates with the StepOnePlus real-time PCR system (Applied Biosystems). TaqMan Gene Expression Master Mix (Applied Biosystems), TaqMan, and UPL probes (Roche) were used. Primers and probes are listed in Table S5.

In Vivo Luciferase Measurements

Light pulse assay: standard growth medium contained 2 % glucose, 0.5 % L-arginine, 1× Vogel's and 150 μM firefly luciferin. 96-well plates were inoculated with 1.5×10^5 conidia per well and incubated in darkness for 16 hours at 25°C. Plates were then exposed to the indicated light pulse regime. Bioluminescence was recorded in darkness at 25°C with an EnVision Xcite Multilabel Reader.

Antibodies

Polyclonal anti-rabbit antibodies were raised and purified using standard techniques. Pol II Ser5-P was raised against SPT(pS) PSYSPT(pS)PSC. WC2 antibodies were raised against a GST-WC-2 protein expressed in Escherichia coli 65. WC1 rabbit antibodies were raised against the C-terminal peptide CREEMGEHQQGLSV and affinity purified. The cysteinyl residues (C) were added to allow coupling of the peptides to SulfoLink coupling resin for affinity purification of antibodies.

Chromatin Immunoprecipitation (ChIP)

ChIP was performed as described previously66. 400 μl grounded mycelia was resuspended in 1.1 ml ChIP Lysis Buffer (50 mM HEPES pH 7.5, 150 mM NaCl, 1 mM EDTA, 1% Triton X-100, 0.1%, SDS, 0.1% DOC, 1 mM PMSF, 1 μg/ml leupeptin, 1 μg/ml pepstatin A) and sonicated using a Covaris S220X sonicator (180 peak power, 20.0 duty factor, 200 cycles/bursts, for 4 min at 4°C). Total extracts were subjected to ChIP with affinity purified antibodies (~1 μg).

RNA and ChIP Sequencing

cDNA was prepared with NEBNext Ultra RNA Prep kit and NEBNext Multiplex oligos. ChIP DNA libraries were prepared with NEBNext ChIP-Seq Library Prep Reagent Set for Illumina with NEBNext Multiplex oligos. A 2100 Bioanalyser was used for quality control of libraries. Fifty base pairs unpaired sequencing was performed with a HiSeq 2000 at GeneCore EMBL Heidelberg.

Sequencing Data Analysis

Raw reads were mapped to *Neurospora crassa* genome (NC10) using Bowtie68. Three mismatches were allowed and reads mapping to more than one location were discarded. RNA-seq analysis: Gene expression was quantified by counting reads falling into exons. Normalization was carried out using the size factor formula as described69. Pol II (Ser5-P) ChIP-seq analysis: The median of Pol II Ser5-P reads in extragenic regions was used for normalization. If not stated otherwise Pol II Ser5-P occupancy was quantified by the number of reads falling into a 500 bp window centered around the start codon.

Mathematical Modeling

Theory for Regulation of transcriptional Bursting Cycles

We analyze a family of models for transcription factors (TF) that activate transcription by modulating different aspects of transcriptional bursting kinetics: burst amplitude (AM), duration (DM) and frequency (FM) (Figures S1 and 1).

To compare with non-equilibrium models, we first formulate a simple thermodynamic model: a TF reversibly binds to its regulatory site, and the bound state initiates mRNA synthesis by physically recruiting RNA polymerase (RNAP, and other co-factors) at the gene promoter. RNAP recruitment is considered a direct consequence of TF binding and is not modeled explicitly. The transcription dynamics at the cell-population level are governed by the following differential equations:

$$\begin{aligned} \frac{du}{dt} &= -k_{on}uw + k_{off}c \\ \frac{dc}{dt} &= k_{on}uw - k_{off}c \\ \frac{dm}{dt} &= fc - \frac{m}{\tau_m} \end{aligned} \qquad \text{(Equation 14)}$$

where u and c denote the levels of the TF-free and TF-bound promoters, respectively. w is the TF concentration; m the mRNA level; k_{on} and k_{off} denote the association and dissociation rate constants of the TF, respectively; f is the rate constant of productive transcription initiation (RNAP firing rate), and τ_m the mean lifetime of mRNA.

As TF-DNA interaction are highly dynamic in eukaryotic cells, with dwell times on the order of seconds (Voss et al., 2011; Morisaki et al., 2014), we assume that the TF binding reaches equilibrium very rapidly. Therefore, the TF-free and TF-bound promoter levels can be calculated as $u = K_d/(K_d + w)$, $c = w/(K_d + w)$, where $K_d = k_{off}/k_{on}$ (dissociation constant). Equation 14 thus reduces to a first-order differential equation:

$$\frac{dm}{dt} = f\frac{w}{K_d + w} - \frac{m}{\tau_m} \qquad \text{(Equation 15)}$$

The rapid equilibrium approximation for TF binding is also used in the following models.

Solving for the steady state (with constant TF concentration), the mRNA level is

$$m_{EQ} = \tau_m v_{EQ} \qquad \text{(Equation 16)}$$

with the transcription rate

$$v_{EQ} = f\frac{w}{K_d + w} \qquad \text{(Equation 17)}$$

The operating point, defined as the TF concentration at which the transcription rate is half-maximal, is the TF dissociation constant K_d. Thus, the sensitivity of the transcription response to the TF is determined by the TF affinity.

Next, we model a generic transcriptional bursting cycle, consisting of an active state, an inactive (but activatable) state and any number ($N = 1, 2, \ldots$) of refractory states (Figure S1A). We assume that the transcription factor binds to all states with the same dissociation constant K_d. Considering rapid equilibrium for TF binding, the differential equations governing the gene fractions in the different states, x_i, as well as mRNA count, m, are:

$$\begin{aligned}
\frac{dx_A}{dt} &= \left(\frac{1}{\tau_{IB}}\frac{w}{K_d + w} + \frac{1}{\tau_{IU}}\frac{K_d}{K_d + w}\right)\left(1 - x_A - \sum_{j=1}^{N} x_{Rj}\right) - \left(\frac{1}{\tau_{AB}}\frac{w}{K_d + w} + \frac{1}{\tau_{AU}}\frac{K_d}{K_d + w}\right)x_A \\
\frac{dx_{R1}}{dt} &= \left(\frac{1}{\tau_{AB}}\frac{w}{K_d + w} + \frac{1}{\tau_{AU}}\frac{K_d}{K_d + w}\right)x_A - \left(\frac{1}{\tau_{RB1}}\frac{w}{K_d + w} + \frac{1}{\tau_{RU1}}\frac{K_d}{K_d + w}\right)x_{R1} \\
\frac{dx_{Rj}}{dt} &= \left(\frac{1}{\tau_{RBj-1}}\frac{w}{K_d + w} + \frac{1}{\tau_{RUj-1}}\frac{K_d}{K_d + w}\right)x_{Rj-1} - \left(\frac{1}{\tau_{RBj}}\frac{w}{K_d + w} + \frac{1}{\tau_{RUj}}\frac{K_d}{K_d + w}\right)x_{Rj}, \quad j = 2, \ldots, N \\
\frac{dm}{dt} &= \left(f_B\frac{w}{K_d + w} + f_U\frac{K_d}{K_d + w}\right)x_A - \frac{m}{\tau_m}
\end{aligned} \qquad \text{(Equation 18)}$$

τ_{IB}, τ_{AB} and τ_{RBj} denote, respectively, the lifetimes of the inactive, active and the j-th refractory promoter states with TF bound; τ_{IU}, τ_{AU} and τ_{RUj} are their TF-free counterparts. f_B and f_U are the transcription initiation rates for the TF-bound and TF-free active promoter states, respectively. If a TF regulates a given step, the corresponding TF-bound and TF-free lifetimes of this state will be different, otherwise they will be identical. We consider three basic regulatory modes for the TF, modulating the transcription initiation rate, the lifetime of the inactive promoter state, or the lifetime of the active promoter state.

First, when a TF controls the transcription initiation rate, we have $f_B = f$ and $f_U = \varepsilon_{AM} f$, whereas $\tau_{IB} = \tau_{IU} = \tau_I$, $\tau_{AB} = \tau_{AU} = \tau_A$ and $\tau_{RBj} = \tau_{RUj} = \tau_{Rj}$. In this regulatory mode, the TF modulates the burst amplitude (AM). We obtain

$$\begin{aligned}
\frac{dx_A}{dt} &= \frac{1}{\tau_I}\left(1 - x_A - \sum_{j=1}^{N} x_{Rj}\right) - \frac{1}{\tau_A}x_A \\
\frac{dx_{R1}}{dt} &= \frac{1}{\tau_A}x_A - \frac{1}{\tau_{R1}}x_{R1} \\
\frac{dx_{Rj}}{dt} &= \frac{1}{\tau_{Rj-1}}x_{Rj-1} - \frac{1}{\tau_{Rj}}x_{Rj}, \quad j = 2, \ldots, N \\
\frac{dm}{dt} &= f\frac{\varepsilon_{AM}K_d + w}{K_d + w}x_A - \frac{m}{\tau_m}
\end{aligned} \qquad \text{(Equation 19)}$$

The mRNA level at steady state is $m = v_{AM}\tau_m$, with the transcription rate

$$v_{AM} = f\frac{\tau_A}{\tau_I + \tau_A + \sum_{j=1}^{N}\tau_{Rj}}\frac{\varepsilon_{AM}K_d + w}{K_d + w} \quad \text{(Equation 20)}$$

If $0 \leq \varepsilon_{AM} < 1$, v_{AM} will be an increasing function of w, and the TF serves as an activator. If $\varepsilon_{AM} > 1$, v_{AM} will decrease with w, and the TF acts as a repressor. The difference between the basal ($w = 0$) and maximum/minimum ($w \to \infty$) transcription rate yields the dynamic range of transcriptional control:

$$\Delta_{AM} = f\frac{\tau_A}{\tau_I + \tau_A + \sum_{j=1}^{N}\tau_{Rj}}|1 - \varepsilon_{AM}| \quad \text{(Equation 21)}$$

The operating point is the transcription factor concentration at which the transcription rate is halfway between basal and maximal, yielding

$$\Omega_{AM} = K_d. \quad \text{(Equation 22)}$$

Second, a TF controlling the lifetime of the inactive promoter state modulates burst frequency (FM). We take $\tau_{IB} = \tau_I$ and $\tau_{IU} = \tau_I/\varepsilon_{FM}$, as well as $f_B = f_U = f$, $\tau_{AB} = \tau_{AU} = \tau_A$ and $\tau_{RBj} = \tau_{RUj} = \tau_{Rj}$. We get

$$\begin{aligned}\frac{dx_A}{dt} &= \frac{1}{\tau_{FM}}\frac{\varepsilon_{FM}K_d + w}{K_d + w}\left(1 - x_A - \sum_{j=1}^{N}x_{Rj}\right) - \frac{1}{\tau_A}x_A\\ \frac{dx_{R1}}{dt} &= \frac{1}{\tau_A}x_A - \frac{1}{\tau_{R1}}x_{R1}\\ \frac{dx_{Rj}}{dt} &= \frac{1}{\tau_{Rj-1}}x_{Rj-1} - \frac{1}{\tau_{Rj}}x_{Rj}, \quad j = 2 \text{ to } N\\ \frac{dm}{dt} &= fx_A - \frac{m}{\tau_m}\end{aligned} \quad \text{(Equation 23)}$$

The steady-state transcription rate is

$$v_{FM} = f\frac{\tau_A}{\tau_I + \tau_A + \sum_{j=1}^{N}\tau_{Rj}}\frac{\varepsilon_{FM}K_d + w}{K_d\frac{\tau_I + \varepsilon_{FM}\left(\tau_A + \sum_{j=1}^{N}\tau_{Rj}\right)}{\tau_I + \tau_A + \sum_{j=1}^{N}\tau_{Rj}} + w}, \quad \text{(Equation 24)}$$

with the dynamic range

$$\Delta_{FM} = f\frac{\tau_A}{\tau_I + \tau_A + \sum_{j=1}^{N}\tau_{Rj}}\frac{|1 - \varepsilon_{FM}|\tau_I}{\tau_I + \varepsilon_{FM}\left(\tau_A + \sum_{j=1}^{N}\tau_{Rj}\right)}. \quad \text{(Equation 25)}$$

Again, these expressions allow for the TF to act either as an activator ($0 \leq \varepsilon_{FM} < 1$) or as a repressor ($\varepsilon_{FM} > 1$). In any case, the operating point of the FM model is:

$$\Omega_{FM} = K_d\frac{\tau_I + \varepsilon_{FM}\left(\tau_A + \sum_{j=1}^{N}\tau_{Rj}\right)}{\tau_I + \tau_A + \sum_{j=1}^{N}\tau_{Rj}}, \quad \varepsilon_{FM} \neq 1 \quad \text{(Equation 26)}$$

The kinetics of the promoter-state transitions determine how sensitively the gene responds to the TF. If $0 \leq \varepsilon_{FM} < 1$, the TF accelerates the transition from the inactive state into the transcriptionally active state and hence acts as an activator. Then we have $\Omega_{FM} < K_d$: the responsiveness of a gene to a TF modulating burst frequency is not limited by the TF affinity. If $\varepsilon_{FM} > 1$, binding of the TF slows the transition into the active state, hence the TF acts as a repressor. Then $\Omega_{FM} > K_d$.

Burst frequency modulation could also be achieved by a TF controlling the lifetime of a refractory promoter state. Equations 23–26 theory carry over to this case in a straightforward manner, simply by swapping τ_I and τ_{Rj}. We will include this case in the model inference from data (see below).

Finally, a TF modulating the lifetime of the active gene state modulates burst duration (DM). We take $\tau_{AB} = \tau_A$ and $\tau_{AU} = \varepsilon_{DM}\tau_A$. For the other parameters we assume $f_B = f_U = f$, $\tau_{IB} = \tau_{IU} = \tau_I$ and $\tau_{RBj} = \tau_{RUj} = \tau_{Rj}$. The dynamics of the DM model are governed by:

$$\begin{aligned}\frac{dx_A}{dt} &= \frac{1}{\tau_I}\left(1 - x_A - \sum_{j=1}^{N} x_{Rj}\right) - \frac{1}{\tau_A}\frac{K_d/\varepsilon_{DM} + w}{K_d + w}x_A \\ \frac{dx_{R1}}{dt} &= \frac{1}{\tau_A}\frac{K_d/\varepsilon_{DM} + w}{K_d + w}x_A - \frac{1}{\tau_{R1}}x_{R1} \\ \frac{dx_{Rj}}{dt} &= \frac{1}{\tau_{Rj-1}}x_{Rj-1} - \frac{1}{\tau_{Rj}}x_{Rj}, \quad j = 2 \text{ to } N \\ \frac{dm}{dt} &= f x_A - \frac{m}{\tau_m}\end{aligned} \qquad \text{(Equation 27)}$$

The steady-state transcription rate, the dynamic range and the operating point in DM model are, respectively:

$$v_{DM} = f\frac{\tau_A}{\tau_A + \tau_I + \sum_{j=1}^{N}\tau_{Rj}}\frac{K_d + w}{K_d\dfrac{\tau_A + \left(\tau_I + \sum_{j=1}^{N}\tau_{Rj}\right)\Big/\varepsilon_{DM}}{\tau_A + \tau_I + \sum_{j=1}^{N}\tau_{Rj}} + w} \qquad \text{(Equation 28)}$$

$$\Delta_{DM} = f\frac{\tau_A}{\tau_I + \tau_A + \sum_{j=1}^{N}\tau_{Rj}}\frac{|1 - 1/\varepsilon_{DM}|\left(\tau_I + \sum_{j=1}^{N}\tau_{Rj}\right)}{\tau_A + \left(\tau_I + \sum_{j=1}^{N}\tau_{Rj}\right)\Big/\varepsilon_{DM}} \qquad \text{(Equation 29)}$$

$$\Omega_{DM} = K_d\frac{\tau_A + \left(\tau_I + \sum_{j=1}^{N}\tau_{Rj}\right)\Big/\varepsilon_{DM}}{\tau_A + \tau_I + \sum_{j=1}^{N}\tau_{Rj}}, \quad \varepsilon_{DM} \neq 1 \qquad \text{(Equation 30)}$$

For $0 \leq \varepsilon_{DM} < 1$, the TF is an activator because it inhibits the transition of the active gene state into the refractory state(s). Then we have $\Omega_{DM} > K_d$. For $\varepsilon_{DM} > 1$, the TF destabilizes the active state and hence acts as a repressor, with $\Omega_{DM} < K_d$.

Equations 26 and 30 suggest a general rule for the location of the operating point. If a TF accelerates the transcriptional bursting cycle, then $\Omega < K_d$: The gene will be more sensitive to accelerating TFs than in the thermodynamic case (equilibrium binding and AM models, where $\Omega = K_d$). Conversely, if the TF puts a brake on the bursting cycle, $\Omega > K_d$: The gene will be less sensitive to braking TFs than in the thermodynamic case. This is indeed true. Consider the average times for the completion of the TF-bound bursting cycle and the TF-free bursting cycle T_{bound} and T_{free}, respectively. For example, for FM (Equation 23), we have $T_{bound} = \tau_I + \tau_A + \sum_{j=1}^{N}\tau_{Rj}$ and $T_{free} = \tau_I/\varepsilon_{FM} + \tau_A + \sum_{j=1}^{N}\tau_{Rj}$. Let $R_{bound,i}$ and $R_{free,i}$ denote the fraction of time spent in gene state i in the TF-bound cycle and the TF-free cycle, respectively. For example, for FM, the fractional times spent in the inactive state are $R_{bound,I} = \tau_I/T_{bound}$ and $R_{free,I} = \tau_I/(\varepsilon_{FM}T_{free})$. With these notations, we get the following general expression for the operating point:

$$\Omega_i = \frac{R_{bound,i}}{R_{free,i}}K_d, \qquad \text{(Equation 31)}$$

where i denotes the state in the bursting cycle whose lifetime is controlled by the TF (specifically, i = I for FM and i = A for DM). Besides FM and DM, this equation also holds for AM, as here $R_{bound,A} = R_{free,A}$ — the TF does not affect cycle duration. Equation 31 shows in general terms that thermodynamic behavior ($\Omega = K_d$) is obtained when the TF does not regulate the duration of the bursting cycle but rather the initiation rate from the active state, while both cycle-accelerating and braking TFs have operating points that deviate from the thermodynamic behavior: Accelerators have $\Omega < K_d$ and brakes have $\Omega > K_d$. These arguments are true regardless of whether the TF functions as an activator or a repressor.

Combinations of FM, AM and DM Mediated by a Transcriptional Activator

Next, we derive two special models that will be used in the analysis of the experimental data, the random telegraph model (no refractory state) and the refractory-cycling model with a single refractory state. At the same time, we generalize to account for all possible modes of TF function simultaneously as we do not know a priori which modes play a role in the data, considering an activating TF. For simplicity, we assume the basal transcription rates in the absence of TF to be zero for AM and FM.

To write the general random telegraph model, we introduce three binary integers, α_{FM}, α_{DM} and α_{AM}, that are 1 when the respective mode of regulation is present and zero otherwise:

$$\frac{dx_A}{dt} = \frac{1}{\tau_I}\left(1 - \alpha_{FM}\frac{K_d}{K_d + w}\right)(1 - x_A) - \frac{1}{\tau_A}\left(1 - \alpha_{DM}\frac{w}{K_d + w}\right)x_A$$
$$\frac{dm}{dt} = f\left(1 - \alpha_{AM}\frac{K_d}{K_d + w}\right)x_A - \frac{m}{\tau_m} \quad \text{(Equation 32)}$$

Note that the activating TF acts to decrease the lifetime of the inactive state (if $\alpha_{FM} = 1$) but increase the lifetime of the active state (if $\alpha_{DM} = 1$).

Similarly, we write the refractory-cycling model with the four binary integers, $\beta_{FM,I}$ (FM via activating the I → A transition), $\beta_{FM,R}$ (FM via activating the R → I transition), β_{DM} and β_{AM}:

$$\frac{dx_A}{dt} = \frac{1}{\tau_I}\left(1 - \beta_{FM,I}\frac{K_d}{K_d + w}\right)(1 - x_A - x_R) - \frac{1}{\tau_A}\left(1 - \beta_{DM}\frac{w}{K_d + w}\right)x_A$$
$$\frac{dx_R}{dt} = \frac{1}{\tau_A}\left(1 - \beta_{DM}\frac{w}{K_d + w}\right)x_A - \frac{1}{\tau_R}\left(1 - \beta_{FM,R}\frac{K_d}{K_d + w}\right)x_R \quad \text{(Equation 33)}$$
$$\frac{dm}{dt} = f\left(1 - \beta_{AM}\frac{K_d}{K_d + w}\right)x_A - \frac{m}{\tau_m},$$

again with $\beta_i = 1$ when the respective mode of regulation is present and zero otherwise.

If the TF modulates a single transcription step, the gene regulatory function has the similar form to the Michaelis-Menten equation (see the analytical expressions for the operating point and dynamic range in Table S1). Of note, with multiple regulatory functions of the TF the gene-regulatory functions contain higher powers of its concentration and hence may be sigmoidal. As an example, we give the steady state expression for the transcription rate in the refractory-cycling model with combined AM and FM:

$$v_{FM-AM} = f\frac{\tau_A w^2}{(\tau_A + \tau_I + \tau_R)w^2 + (\tau_A + 2\tau_I + \tau_R)K_d w + \tau_I K_d^2}. \quad \text{(Equation 34)}$$

Speed of the Transcriptional Response

Next, we examine how rapidly a gene responds to a step elevation on TF activity. We consider the response time $\tau_{response}$, defined as the time at which the mRNA is halfway between basal level and steady state.

For equilibrium-binding and AM models, the mRNA response to a TF step from 0 to w has the form

$$m_{AM}(t) = m_{AM}(\infty)\left(1 - e^{-t/\tau_m}\right) \quad \text{(Equation 35)}$$

for all AM models (Equations 32 and 33) as well as the equilibrium-binding model (Equation 15). Here $m_{AM}(\infty)$ denotes the steady-state mRNA level that is eventually reached, where

$$m_{AM}(\infty) = \begin{cases} \tau_m \tilde{f}(w) & \text{Equilibrium-binding model} \\ \tau_m \tilde{f}(w)\dfrac{\tau_A}{\tau_A + \tau_I} & \text{Random telegraph model} \\ \tau_m \tilde{f}(w)\dfrac{\tau_A}{\tau_A + \tau_I + \tau_R} & \text{Refractory-cycling model} \end{cases} \quad \text{(Equation 36)}$$

and $\tilde{f}(w) = fw/(K_d + w)$ is the TF dependent transcription initiation rate. Although different models show different mRNA steady state, they all share the same response time:

$$\tau^{AM}_{response} = \tau_m \ln 2 \quad \text{(Equation 37)}$$

implying that speed of gene induction is limited by a parameter unrelated to transcription itself, namely the lifetime of mRNA.

In practice, there may be further contributions to the response time from transcription initiation (including changes in chromatin structure), elongation and splicing of the transcript (which do not enter Equation 37 because of simplifying assumptions in the model, such as rapid binding equilibrium for the TF and fast recruitment of RNAP). mRNA lifetime is often greater than these contributions and will then dominate the response time, so that Equation 37 holds approximately. For example, in a human cell line, the median mRNA lifetime is 9 h (Schwanhausser et al., 2011), compared with an estimated elongation time of 10-20 min for a human gene of

median length (24 kbp) and a typical delay of 10-30 min when mRNA appears in the cytoplasm of mammalian cells after the start of transcription (Ben-Ari et al., 2010).

For the FM telegraph model, we find the following mRNA response:

$$m_{\mathrm{FM-TG}}(t) = m_{\mathrm{FM-TG}}(\infty)\left[1 - \frac{\tau_{\mathrm{m}}}{\tau_{\mathrm{m}} - \tau_{\mathrm{B}}(w)} e^{-\frac{t}{\tau_{\mathrm{m}}}} + \frac{\tau_{\mathrm{B}}(w)}{\tau_{\mathrm{m}} - \tau_{\mathrm{B}}(w)} e^{-\frac{t}{\tau_{\mathrm{B}}(w)}}\right] \quad \text{(Equation 38)}$$

As the TF controls the rate of the I → A transition, we define the following TF-dependent lifetime of the inactive state

$$\tilde{\tau}_{\mathrm{I}}(w) = \tau_{\mathrm{I}} \frac{K_{\mathrm{d}} + w}{w} \quad \text{(Equation 39)}$$

Then, in Equation 38, we have the steady-state mRNA level:

$$m_{\mathrm{FM-TG}}(\infty) = \tau_{\mathrm{m}} f \frac{\tau_{\mathrm{A}}}{\tau_{\mathrm{A}} + \tilde{\tau}_{\mathrm{I}}(w)} \quad \text{(Equation 40)}$$

and the TF-dependent time constant:

$$\tau_{\mathrm{B}}(w) = \frac{\tau_{\mathrm{A}} \tilde{\tau}_{\mathrm{I}}(w)}{\tau_{\mathrm{A}} + \tilde{\tau}_{\mathrm{I}}(w)} \quad \text{(Equation 41)}$$

The telegraph DM model yields:

$$m_{\mathrm{DM-TG}}(t) = m_{\mathrm{DM-TG}}(\infty)\left\{1 - \frac{\tau_{\mathrm{I}}\tau_{\mathrm{m}}}{[\tilde{\tau}_{\mathrm{A}}(w) + \tau_{\mathrm{I}}](\tau_{\mathrm{m}} - \tau_{\mathrm{I}})} e^{-\frac{t}{\tau_{\mathrm{m}}}} + \frac{\tau_{\mathrm{I}}^2}{[\tilde{\tau}_{\mathrm{A}}(w) + \tau_{\mathrm{I}}](\tau_{\mathrm{m}} - \tau_{\mathrm{I}})} e^{-\frac{t}{\tau_{\mathrm{I}}}}\right\} \quad \text{(Equation 42)}$$

where we similarly introduce the TF-dependent lifetime of the active state:

$$\tilde{\tau}_{\mathrm{A}}(w) = \tau_{\mathrm{A}} \frac{K_{\mathrm{d}} + w}{K_{\mathrm{d}}} \quad \text{(Equation 43)}$$

yielding the steady state level

$$m_{\mathrm{DM-TG}}(\infty) = \tau_{\mathrm{m}} f \frac{\tilde{\tau}_{\mathrm{A}}(w)}{\tilde{\tau}_{\mathrm{A}}(w) + \tau_{\mathrm{I}}} \quad \text{(Equation 44)}$$

For both solutions (Equations 38 and 42), the mRNA level increases monotonically with time (which can be shown analytically be demonstrating that time derivatives are always larger than zero). The response is, in general, slower than the mRNA turnover due to the time delay in dynamic transitions between promoter states. Fast promoter switching could accelerate gene induction, but the speed is still limited by the lifetime of mRNA.

From a mathematical viewpoint, the telegraph model uses only one degree of freedom to describe gene induction, which inevitably gives rise to monotonic transcription response. The refractory-cycling model adds another degree of freedom (the occupancy of the refractory state). As we will see below, this allows for a transcriptional overshoot when the I → A transition is regulated. The gene activity first rises abruptly upon promoter activation, then decreases due to refractoriness, and finally relaxes to the steady state.

The FM refractory-cycling model can be solved for the gene-induction dynamics, but the analytical expressions are not intuitive. As described in the main text, an overshoot of transcription rate is a typical behavior in this model. We now present a simple model of how overshooting transcription rate affects the mRNA response time. To this end, we approximate the promoter activity by a step function (see Figure S3):

$$\frac{dm}{dt} = v(t) - \frac{m}{\tau_{\mathrm{m}}}$$
$$v(t) = \begin{cases} v_{\mathrm{T}} & 0 \le t \le T \\ v_{\mathrm{S}} & t \ge T \end{cases} \quad \text{(Equation 45)}$$

where v_{T} is the population-level transcription initiation rate in the transient phase of promoter activity, and v_{S} the rate at steady state (both proportional to the fraction of promoters in the active state). T denotes the duration of the transient phase. Then

$$m(t) = \begin{cases} v_{\mathrm{T}}\tau_{\mathrm{m}}\left(1 - e^{-\frac{t}{\tau_{\mathrm{m}}}}\right) & 0 \le t < T \\ v_{\mathrm{S}}\tau_{\mathrm{m}} - v_{\mathrm{T}}\tau_{\mathrm{m}} e^{-\frac{t}{\tau_{\mathrm{m}}}} + \tau_{\mathrm{m}}(v_{\mathrm{T}} - v_{\mathrm{S}}) e^{-\frac{t-T}{\tau_{\mathrm{m}}}} & t \ge T \end{cases} \quad \text{(Equation 46)}$$

If the mRNA lifetime is sufficiently long, mRNA levels will not overshoot but approach the steady state monotonically (Figure S3). In this informative case, the usual definition of response time remains meaningful. As the analytical solution consists of two (continuous) branches, we need to consider two cases: mRNA reaches half its steady-state level (i) on the first branch ($t < T$) or (ii) on the second branch ($t \geq T$). The critical condition setting apart these two cases is when mRNA attains half its steady state exactly at T:

$$m(T) = \frac{1}{2} v_S \tau_m \qquad \text{(Equation 47)}$$

defining the critical duration of the overshooting transient relative to mRNA lifetime as

$$T^* = \tau_m \ln \frac{2}{2 - v_S/v_T} \qquad \text{(Equation 48)}$$

The respective response times are:

$$\tau_{response} = \begin{cases} \tau_m \ln \dfrac{2}{2 - v_S/v_T} & T \geq T^* \quad \text{(case i)} \\ \tau_m \ln \dfrac{2 - 2(1 - v_S/v_T)e^{T/\tau_m}}{v_S/v_T} & T < T^* \quad \text{(case ii)} \end{cases} \qquad \text{(Equation 49)}$$

In the first case the response time can be arbitrarily fast as the transcriptional overshoot becomes larger; we have $\lim_{v_S/v_T \to 0} \tau_{response} = 0$ if $T \geq T^*$. In the telegraph model, increasing the rate of transcription would not speed up the response because the steady state would also increase.

Model Selection and Parameter Inference

To confront our theory with experimental data, we utilized the light-controlled transcription system in *Neurospora crassa*. The White Collar Complex (WCC) is the main photoreceptor and GATA type transcriptional activator in response to blue light. This system allows us to quantify, at the population level, the dynamics of the transcriptional activator binding, mRNA production and activity of luciferase reporter for light-controlled genes using single light pulse (LP) and double LPs with varied inter-LP intervals and light intensities (Cesbron et al., 2015). We systematically enumerated all possible models that combine different bursting modes (telegraph or refractory-cycling) and distinct WCC modulation manners (AM, DM and FM) and fitted them to multiple sets of time-resolved data for two key WCC target genes, *frequency* (*frq*) and *vivid* (*vvd*).

The data-driven model for light-controlled transcription in *Neurospora crassa* consists of three modules: (1) light-controlled WCC activation and inactivation, (2) promoter-state transitions and (3) transcriptional output (i.e. mRNA and luciferase reporter), as shown in Figure S5A.

In the first module, WCC has three main states: dark, light and phosphorylation. The dark form WCC prevails in the absence of light, and is produced at a constant rate. Dark form WCC senses light (via the LOV domain) and switches to the light form, with a rate that is proportional to the light intensity. The light form WCC is then deactivated via phosphorylation. Dark and phosphorylated forms are degraded (degradation of the light form was also considered in the model but the turnover rate was consistently fit as zero). The equations governing the kinetics of WCC inactivation-activation are:

$$\begin{aligned} \frac{dw_D}{dt} &= v - \frac{1}{\tau_{wd}} w_D - k_{wa} s(t) w_D \\ \frac{dw_L}{dt} &= k_{wa} w_D s(t) - \frac{1}{\tau_{phos}} w_L \\ \frac{dw_P}{dt} &= \frac{1}{\tau_{phos}} w_L - \frac{1}{\tau_{wp}} w_P \end{aligned} \qquad \text{(Equation 50)}$$

where v and τ_{wd} are the production rate and mean lifetime of dark form WCC, respectively. $k_{wa}s(t)$ is the rate constant for WCC transiting from dark to light form, where $s(t)$ is the time-dependent light signal. τ_{phos} is the characteristic time for WCC phosphorylation (or the mean lifetime of the unphosphorylated light form WCC). τ_{wp} is the mean lifetime of the phosphorylated WCC.

In the second module of promoter-state transition, we will consider both random telegraph and refractory-cycling models. Both light form and phosphorylated WCC are assumed to bind to their regulatory sites on the DNA – light responsive elements (LRE) – with the same K_d, but only the bound light-form WCC acts in transcription. Hence the promoter activity in the telegraph model is:

$$\frac{dx_A}{dt} = \frac{1}{\tau_I}(1 - \alpha_{FM}\Phi)(1 - x_A) - \frac{1}{\tau_A}[1 - \alpha_{DM}(1 - \Phi)]x_A \qquad \text{(Equation 51)}$$

and the refractory-cycling model reads:

$$\begin{aligned} \frac{dx_A}{dt} &= \frac{1}{\tau_I}(1 - \beta_{FM,I}\Phi)(1 - x_A - x_R) - \frac{1}{\tau_A}[1 - \beta_{DM}(1 - \Phi)]x_A \\ \frac{dx_R}{dt} &= \frac{1}{\tau_A}[1 - \beta_{DM}(1 - \Phi)]x_A - \frac{1}{\tau_R}(1 - \beta_{FM,R}\Phi)x_R \end{aligned} \qquad \text{(Equation 52)}$$

where

$$\Phi = \frac{K_d + w_P}{K_d + w_L + w_P} \quad \text{(Equation 53)}$$

The third module of the models describes the dynamics of endogenous (*frq* and *vvd*) mRNA and luciferase reporter mRNA as well as luciferase protein:

$$\begin{aligned} \frac{dm}{dt} &= v_0 + k_m(1 - \beta_{AM}\Phi)x_A - \frac{1}{\tau_m}m \\ \frac{dm_L}{dt} &= v_{0L} + k_{mL}(1 - \beta_{AM}\Phi)x_A - \frac{1}{\tau_{mL}}m_L \\ \frac{dl}{dt} &= k_L m_L - \frac{1}{\tau_L}l \end{aligned} \quad \text{(Equation 54)}$$

where m and m_L denote the concentrations of genomic mRNA and luciferase mRNA, respectively, and l that of the luciferase protein. In the dark, *frq* and *vvd* show basal transcription activity not mediated by LRE, which is modeled by a constant mRNA production rate, v_0 for genomic mRNA and v_{0L} for luciferase mRNA. The transcription initiation rate of an active promoter is k_m for genomic mRNA, and k_{mL} for luciferase mRNA. The mean lifetime of endogenous mRNA τ_m is gene specific, whereas the lifetime of luciferase mRNA τ_{mL} is the same for distinct promoters. The luciferase protein is synthesized with rate constant k_L, and its mean lifetime is τ_L.

Quantitative RT-PCR quantifies the relative level of mRNA, but not the absolute mRNA concentration. In addition, the luciferase activity also requires a scaling factor to link the experimental readout to the actual protein concentration. To compare these data directly with the models, we divided both sides of Equation 54 by the corresponding basal levels in the absence of light stimulus ($w_L = w_P = 0$) for genomic mRNA, luciferase mRNA and luciferase protein:

$$\begin{aligned} m_D &= \tau_m[v_0 + k_m(1 - \beta_{AM})x_{AD}] \\ m_{LD} &= \tau_{mL}[v_{0L} + k_{mL}(1 - \beta_{AM})x_{AD}] \\ l_D &= k_L\tau_L m_{LD} \end{aligned} \quad \text{(Equation 55)}$$

where x_{AD} is the level of active promoter in the dark. Then Equation 54 becomes:

$$\begin{aligned} \frac{dM}{dt} &= \frac{1}{\tau_m}\left[1 + f\frac{(1 - \beta_{AM}\Phi)x_A - (1 - \beta_{AM})x_{AD}}{1 + f(1 - \beta_{AM})x_{AD}} - M\right] \\ \frac{dM_L}{dt} &= \frac{1}{\tau_{mL}}\left[1 + \eta f\frac{(1 - \beta_{AM}\Phi)x_A - (1 - \beta_{AM})x_{AD}}{1 + \eta f(1 - \beta_{AM})x_{AD}} - M_L\right] \\ \frac{dL}{dt} &= \frac{1}{\tau_L}(M_L - L) \end{aligned} \quad \text{(Equation 56)}$$

where $M = m/m_D$, $M_L = m_L/m_{LD}$ and $L = l/l_D$. The genomic mRNA production rate is $f = k_m/v_0$, and the luciferase mRNA production rate is ηf, where $\eta = \frac{k_{mL}}{v_{0L}}/\frac{k_m}{v_0}$. These two rates reflect fold change in transcription rate.

While Equation 56 contains all possible models, most models actually have a simpler form since the bursting kinetics shuts down without active WCC (in the dark). Examples are shown in Figure S1: T1 and T3 – T7 for telegraph model, R1 – R2 and R4 – R15 for refractory-cycling model. These models are described by:

$$\begin{aligned} \frac{dM}{dt} &= \frac{1}{\tau_m}[1 + f(1 - \beta_{AM}\Phi)x_A - M] \\ \frac{dM_L}{dt} &= \frac{1}{\tau_{mL}}[1 + \eta f(1 - \beta_{AM}\Phi)x_A - M_L] \\ \frac{dL}{dt} &= \frac{1}{\tau_L}(M_L - L) \end{aligned} \quad \text{(Equation 57)}$$

Two models in Figure S1, T2 and R3, still show slow promoter transitions even in the absence of active WCC:

$$\begin{aligned} \frac{dM}{dt} &= \frac{1}{\tau_m}\left[1 + f\frac{x_A - x_{AD}}{1 + fx_{AD}} - M\right] \\ \frac{dM_L}{dt} &= \frac{1}{\tau_{mL}}\left[1 + \eta f\frac{x_A - x_{AD}}{1 + \eta fx_{AD}} - M_L\right] \\ \frac{dL}{dt} &= \frac{1}{\tau_L}(M_L - L). \end{aligned} \quad \text{(Equation 58)}$$

The binary factors α_i and β_i allow us to enumerate all possible models with distinct TF actions (AM, FM and DM). For the telegraph model, the TF can in principle control one or combinations of the 3 bursting parameters (τ_I, τ_A and f), therefore the number of all possible models is $2^3 - 1 = 7$, where we exclude the model without any TF action. The refractory-cycling model generates $2^4 - 1 = 15$ regulation modes. Taken together, for a single gene, there are potentially 7 + 15 = 22 models; and for two co-regulated genes (by WCC) *frq* and *vvd*, the total number of models is $22^2 = 484$.

All 484 models were fitted to a comprehensive dataset for *frq* an *vvd*, including kinetics of WCC occupancy, genomic mRNA and luciferase reporter under various light stimulus conditions (Figures 3D–3G). The optimization was performed using the trust-region method to search for the local minimum of the negative log likelihood. To find the global minimum, the initial parameter values were chosen by Latin hypercube sampling (1000 samples for each model). The tasks above were performed using Data2Ddynamic (D2D) framework, a Matlab-based open source package (Raue et al., 2015). We ranked all models by the standard Akaike information criterion (AIC), which penalizes the goodness of fit (log likelihood) by the number of free parameters. As the parameters counts between models vary comparatively little, the result of the model selection is dominated by the goodness of fit. Indeed, model ranking by likelihood values yields the same results as by AIC (Figure S5B). Four best models were selected, and their common features were: (1) both *frq* and *vvd* are refractory; (2) the WCC modulates the burst frequency for both genes.

There are 29 independent parameters in the model for *frq* and *vvd* promoters (details see Table S2). The 95% confidence intervals of these parameters were calculated by using the profile likelihood, as implemented in D2D. Most (27 out of 29) parameters are identifiable (upper and lower confidence bounds); 2 parameters, the mean lifetime of inactive *frq* promoter τ_I^{frq} and the mean lifetime of genomic *vvd* mRNA τ_m^{vvd}, have upper informative bounds (Figure S6, Table S2).

Inference of Transcription Dynamics from Luciferase Time Series

Our theory predicts overshooting mRNA dynamics as a hallmark of transcriptional refractoriness. To test this prediction, we inferred the mRNA dynamics from unstable luciferase (luc_{PEST}) signals of *frq* and *vvd* under constant low light. We fitted the time-resolved luciferase activity using cubic splines, and use the optimized spline and its time derivative to infer the mRNA dynamics based on the following equation:

$$\frac{dL}{dt} = \frac{1}{\tau_L}(m - L) \qquad \text{(Equation 59)}$$

where m and L are the levels of luciferase mRNA and protein, respectively; τ_L is the mean lifetime of the luciferase protein. The mRNA level can be obtained by rearranging the above equation:

$$m = \tau_L \frac{dL}{dt} + L \qquad \text{(Equation 60)}$$

The half-life time of the luciferase used here (luc_{PEST}) is ~25 min (Cesbron et al., 2013), which gives the value for $\tau_L = 25/\ln 2 \approx 36$ min. To avoid the spurious overshoot arising from the cubic spline itself, we constrained the spline to be monotonic. This is a conservative assumption, as the luciferase reporter may indeed overshoot due to its short lifetime.

To test the robustness of the inference on the overshooting kinetics, we took another approach that directly parameterize the mRNA kinetics (rather than the protein level) using a mechanistic model. We used a simple model similar to the one introduced in the section for the response speed of the refractory-cycling model. For computational convenience, we chose a smooth step function to mimic the promoter activity (Figure S7). Three parameters define the step function: the transient level of active promoter v_T, the time duration of the transient phase T and the promoter level at steady state v_S:

$$p = \begin{cases} v_T & 0 \le t < T \\ v_S & t \ge T \end{cases} \qquad \text{(Equation 61)}$$

The kinetics of luciferase mRNA and protein are governed by the following equations:

$$\begin{aligned} \frac{dm}{dt} &= \frac{1}{\tau_m}(1 + fp - m) \\ \frac{dL}{dt} &= \frac{1}{\tau_L}(m - L). \end{aligned} \qquad \text{(Equation 62)}$$

We fixed the value of the lifetime of the luciferase protein τ_L, and the transcription rate constants f for *frq* and *vvd* (taking the values in Table S2). Fitting this model to the same luciferase data used in the previous method yielded again the overshooting dynamics of both *frq* and *vvd* transcription responses, suggesting that these two promoters are intrinsically refractory.

A Model for Chromatin Looping between Enhancer and Promoter

In this section, we extend the refractory-cycling model to link the promoter activation (I → A transition) to dynamic promoter-enhancer interaction via chromatin looping. The gene activation step I → A in the original models is more finely resolved into a chromatin looping step that brings enhancer-bound TF in contact with the gene promoter, followed by promoter activation from the looped configuration (Figure 6A). Specifically, the inactive promoter occurs in two states, unlooped and looped, with lifetimes $\tau_{unlooped}$ and τ_{looped}, respectively. Loop formation is considered a dynamic and reversible process (Fukaya et al., 2016; Bartman et al., 2016). The looped state, with bound activator (WCC), can either switch back to the unlooped state, or undergo an irreversible

transition that activates the promoter for transcription. The kinetics of the latter process are characterized by a new, promoter-specific, time constant τ_O. While in the original model, the population-level gene activation rate is

$$\text{gene activation rate} = \frac{1}{\tau_I} \quad \text{(Equation 63)}$$

this rate becomes in the extended model

$$\text{gene activation rate} = \frac{1}{\tau_o}\,\frac{\tau_{looped}}{\tau_{looped}+\tau_{unlooped}} \quad \text{(Equation 64)}$$

where $\frac{\tau_{looped}}{\tau_{looped}+\tau_{unlooped}}$ is the fraction of the looped promoter state, considering rapid and reversible looping.

Comparing this expression with Equation 63, we obtain:

$$\tau_I = \tau_o \frac{\tau_{looped}+\tau_{unlooped}}{\tau_{looped}} \quad \text{(Equation 65)}$$

This relation expresses the lifetime of the inactive gene state in the previous models in terms of chromatin looping rates and promoter-specific activation from the looped state. It has been reported that the DNA spends much more time in the unlooped state than in the looped state (Chen et al., 2014), so we simplify the above equation using $\tau_{unlooped} \gg \tau_{looped}$:

$$\tau_I = \tau_o\left(1+\frac{\tau_{unlooped}}{\tau_{looped}}\right) \simeq \tau_o \frac{\tau_{unlooped}}{\tau_{looped}} \quad \text{(Equation 66)}$$

The probability of the two sites on chromatin meeting via looping is quantified, using polymer theory, by j_M, the relative concentration of one site with respect to the other. j_M can naturally be linked to the above equation via:

$$\frac{\tau_{unlooped}}{\tau_{looped}} = c^{-1} j_M^{-1}(L) \quad \text{(Equation 67)}$$

where c is a scaling factor that, for our purposes, can be absorbed into the parameter τ_O, yielding

$$\tau_I = \gamma j_M^{-1} \quad \text{(Equation 68)}$$

where $\gamma = \tau_O/c$. Therefore, the gene activation time τ_I is determined by the promoter-specific factor γ and factor j_M, which depends on looping distance. The dependence of j_M on the genomic distance between two sites on the same chromatin L (unit: bp) has been measured (Ringrose et al., 1999) and is well described by the following equation from polymer theory

$$j_M(L,P) = \frac{1.25\times 10^5}{P^3}\left(\frac{4P}{L\times 10^4}\right)^{\frac{3}{2}} \exp\left(-\frac{510P^2}{6.25L^2+50P^2}\right) \quad \text{(Equation 69)}$$

where P is the persistent length of the chromatin (in nm), L is the distance in bp, and j_M is in mol/l. As nucleosome repeat length is the major determinant of chromatin persistence (Ringrose et al., 1999), we adjusted P from the average value measured in human cells (27 nm), with a repeat length of ~200 bp, to *Neurospora* chromatin with a repeat length of ~170 bp, yielding $P = \frac{170}{200}\times 27 \simeq 23\text{nm}$.

Moreover, we have previously estimated τ_I for the WCC target genes *frq* and *vvd*, using the original, simpler models. The measured chromatin looping data together with the inferred τ_I values fix the values of γ for the two genes (Equation 68). Thus the extension of the theory does not introduce new unknown parameters. Instead, it provides a mechanistic interpretation of the gene activation rate that can be tested experimentally by changing promoter-LRE distance (L) and swapping promoters to change τ_O. We have used this theory to predict the dose-response curves for luciferase reporter expression driven by *frq* or *vvd* promoters and LREs at different distances. The prediction confidence bands (95%) of the dose-response curves are estimated by calculating the prediction profile likelihood using the D2D package (Kreutz et al., 2012; Raue et al., 2015).

QUANTIFICATION AND STATISTICAL ANALYSIS

Pairwise tests were performed using two-sample t-test (built-in function in Matlab) for WCC occupancy (by ChIP-PCR, n = 3) and mRNA level (by RT-PCR, n = 3) under different light intensities (Figure 5E), with significance defined as *, $p < 0.05$.

Cell Systems, Volume *6*

Supplemental Information

Frequency Modulation of Transcriptional Bursting Enables Sensitive and Rapid Gene Regulation

Congxin Li, François Cesbron, Michael Oehler, Michael Brunner, and Thomas Höfer

Table of Contents

Supplemental Figures

Figure S1. Model schemes of transcriptional regulation, Related to Figure 1.

Figure S2. Dynamic dose-response follows steady-state dose-response, Related to Figure 2.

Figure S3. Simplified method for analytical solution of transcription response time with overshooting promoter activity, Related to Figure 2 and STAR Methods.

Figure S4. Transcriptional response to the duration of transcription factor activity, Related to Figure 2.

Figure S5. Data-driven modeling of WCC target genes, Related to Figure 3.

Figure S6. Identifiability of inferred parameters by profile likelihood analysis, Related to Figure 3.

Figure S7. Overshoot in mRNA dynamics under constant light, Related to Figure 4 and STAR Methods.

Supplemental Tables

Table S1. Theory predictions on transcriptional regulation at steady state, Related to Figure 2.

Table S2. Parameter inference for frq and vvd, Related to Figure 5.

Table S3. Sequence of the *frqΔLRE* promoter, Related to Figure 6. Mutagenized nucleotides are bolded and underlined.

Table S4. Primers used for *frq* and *vvd* hybrid lucPEST constructs, Related to Figure 6.

Table S5. Primers and probes used for qRT-PCR and ChIP-qPCR, Related to Figure 6.

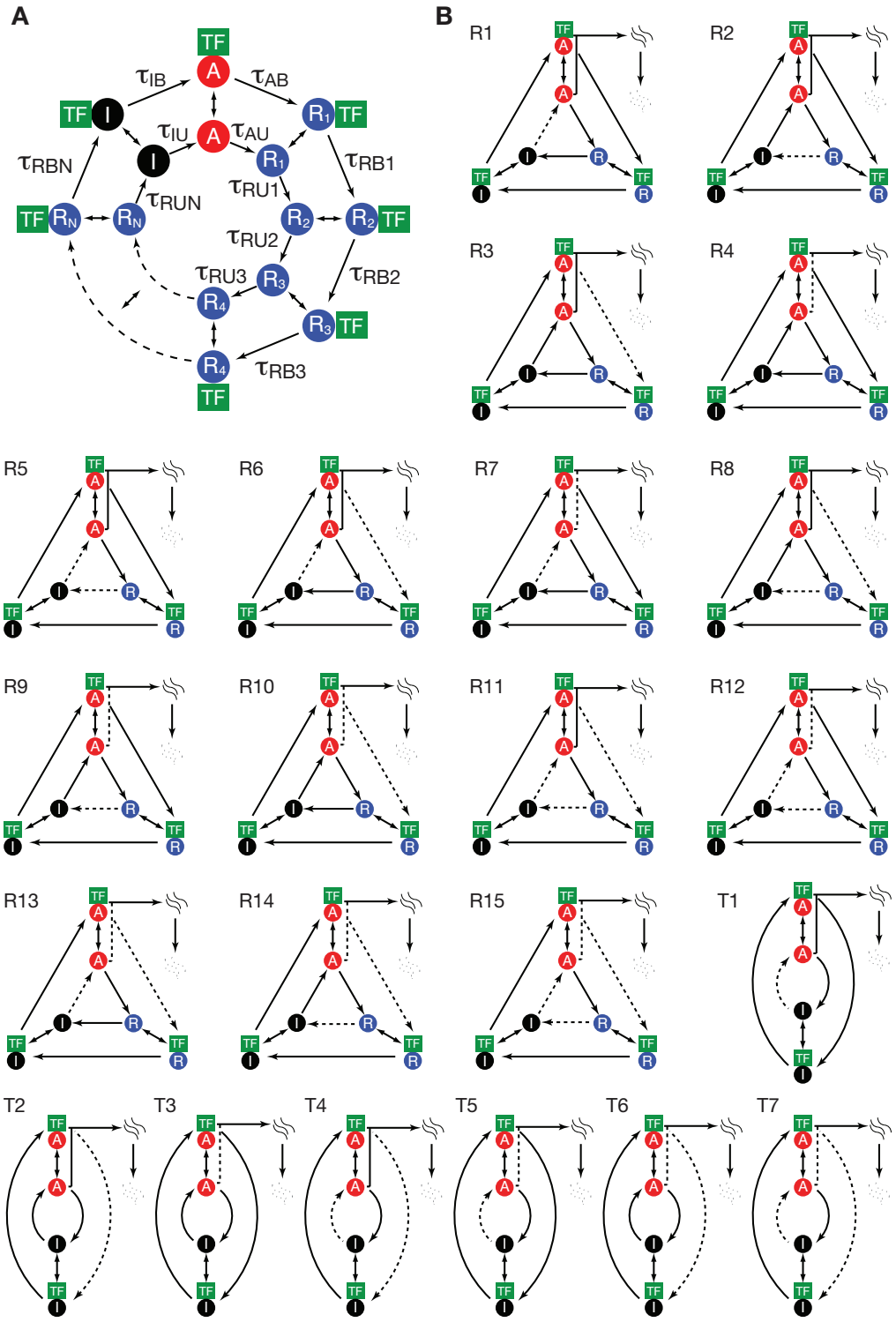

Figure S1. Model schemes of transcriptional regulation, Related to Figure 1. (A) Generic model of transcriptional regulation via modulation of the transcriptional bursting cycle with inactive (I), active (A) and potentially multiple refractory states (R_1, R_2, …). (B) A transcription factor modulates (in an all-or-none manner) a single or multiple steps in refractory-cycling model (denoted by R) and telegraph model (denoted by T).

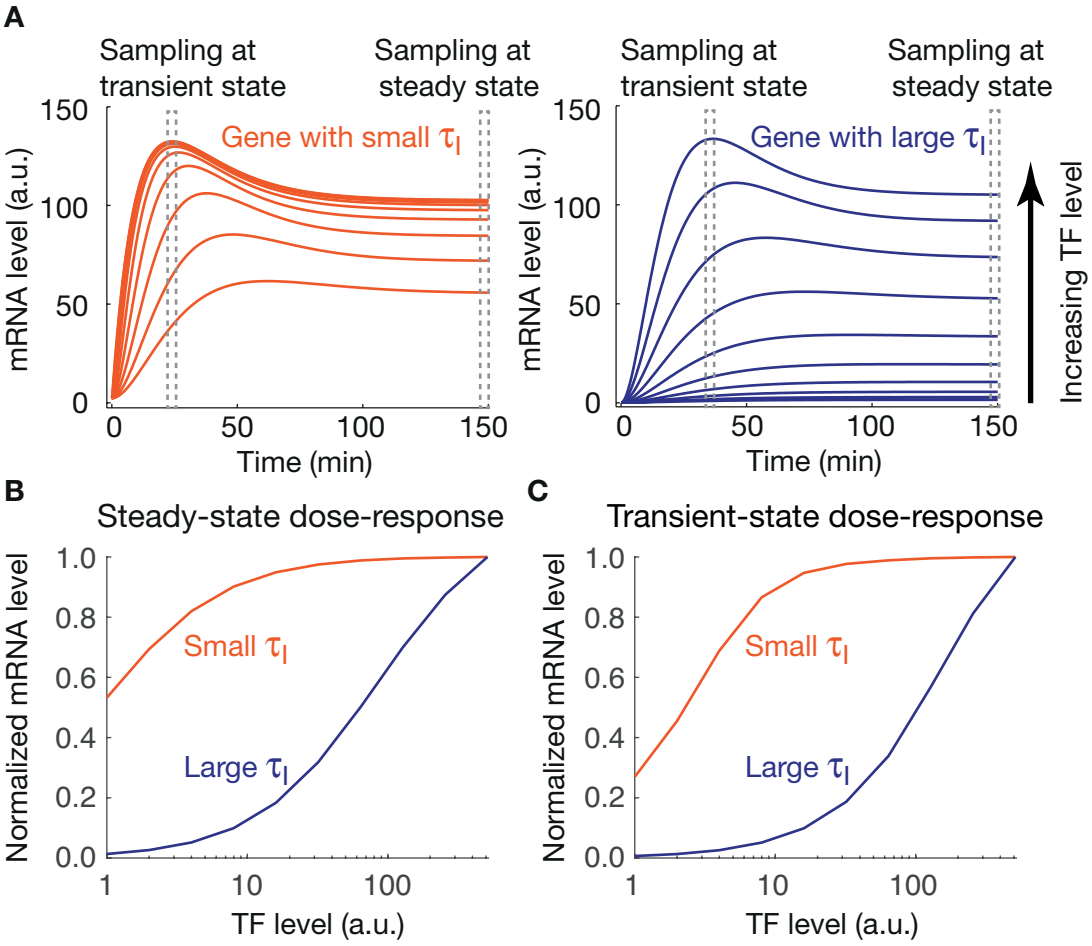

Figure S2. Dynamic dose-response follows steady-state dose-response, Related to Figure 2. (A) Simulations of transcription dynamics of genes with small τ_l (left panel) and large τ_l (right panel) under different TF concentrations. The dose-response can be quantified by transcription outputs at steady state (B) as well as transient state (C). Frequency-modulated refractory cycling model was used for simulation. The parameter values are based on the best fit for *frq* and *vvd* in Table S2.

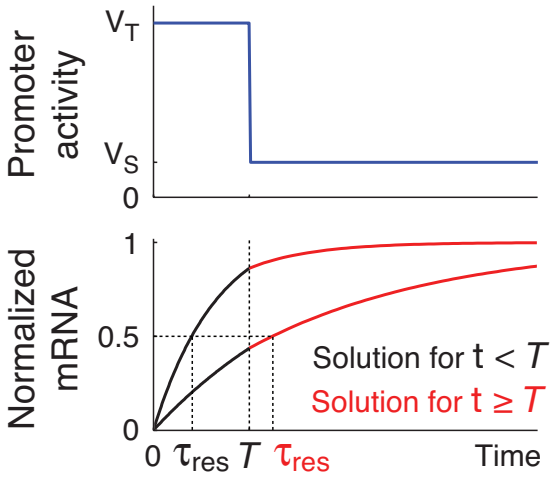

Figure S3. Simplified method for analytical solution of transcription response time with overshooting promoter activity, Related to Figure 2 and STAR Methods. V_T and V_S are the constant transcription rates in the transient and steady-state phases of the promoter activity, respectively, and T is the duration of the overshoot.

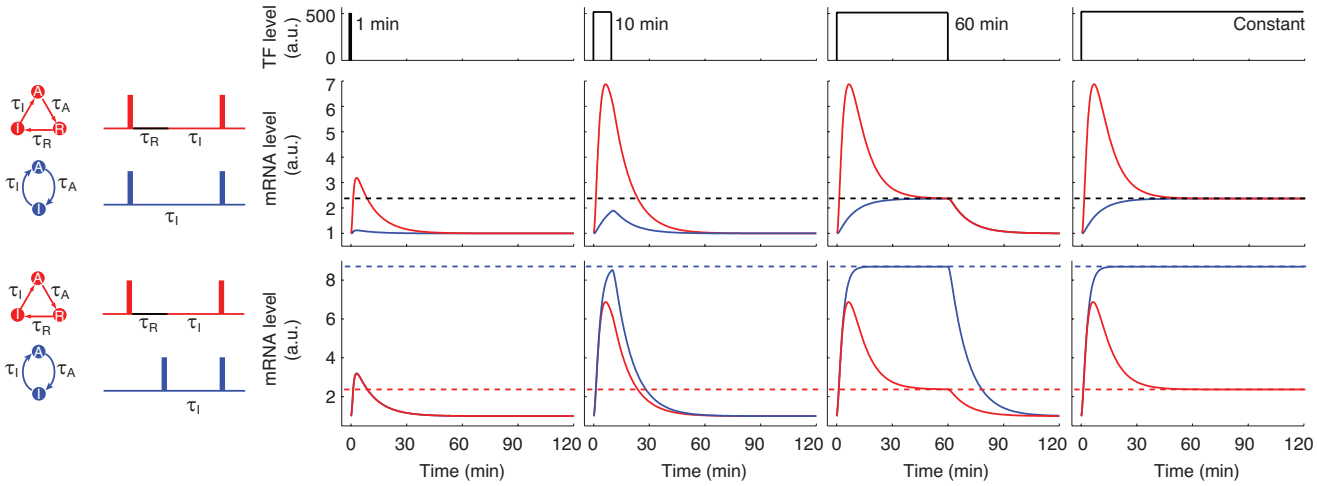

Figure S4. Transcriptional response to the duration of transcription factor activity, Related to Figure 2. The transcription factor is applied (simulated) at a fixed concentration with varying durations: 1, 10 and 60 minutes as well as constant (top row). Responses of refractory-cycling model (red) and random telegraph model (blue) are compared in two scenarios. In the first scenario, both models share the same steady-state mRNA level (middle row, $\tau_I^{\text{telegraph}} = \tau_I^{\text{refractory-cycling}} + \tau_R^{\text{refractory-cycling}}$, with the same τ_A). In the second scenario, the two models show the same initial promoter activation rate ($\tau_I^{\text{telegraph}} = \tau_I^{\text{refractory-cycling}}$, with the same τ_A) but differ in steady state (bottom row). The parameters used for the simulation are those inferred for *frq* (Table S2).

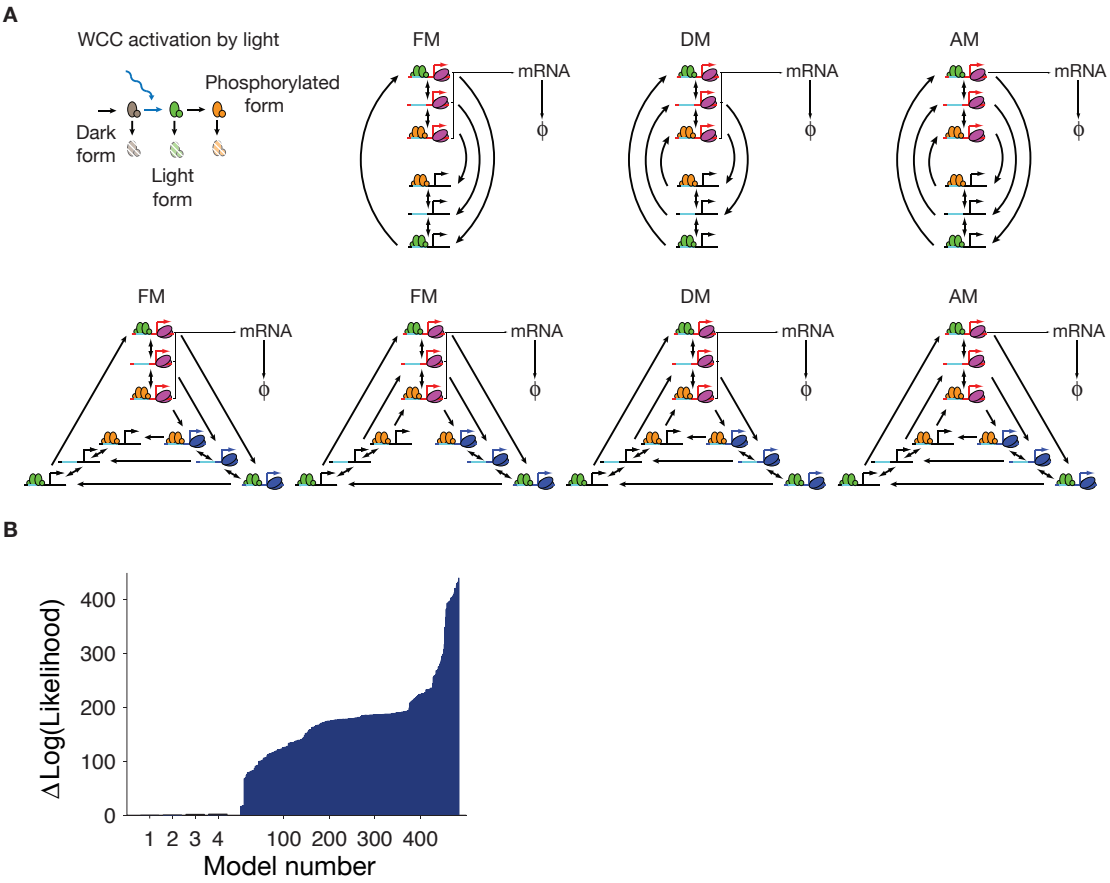

Figure S5. Data-driven modeling of WCC target genes, Related to Figure 3. (A) Basic model schemes of transcriptional regulation by light-controlled WCC. (B) Model ranking by likelihood.

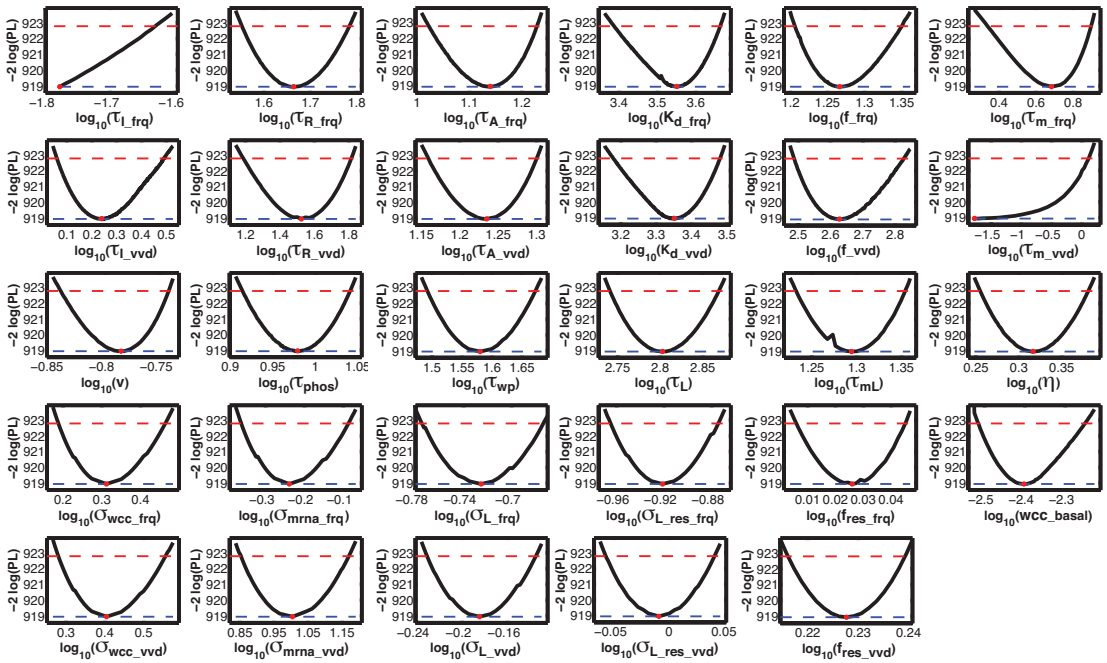

Figure S6. Identifiability of inferred parameters by profile likelihood analysis, Related to Figure 3. Details of the parameters see Table S2.

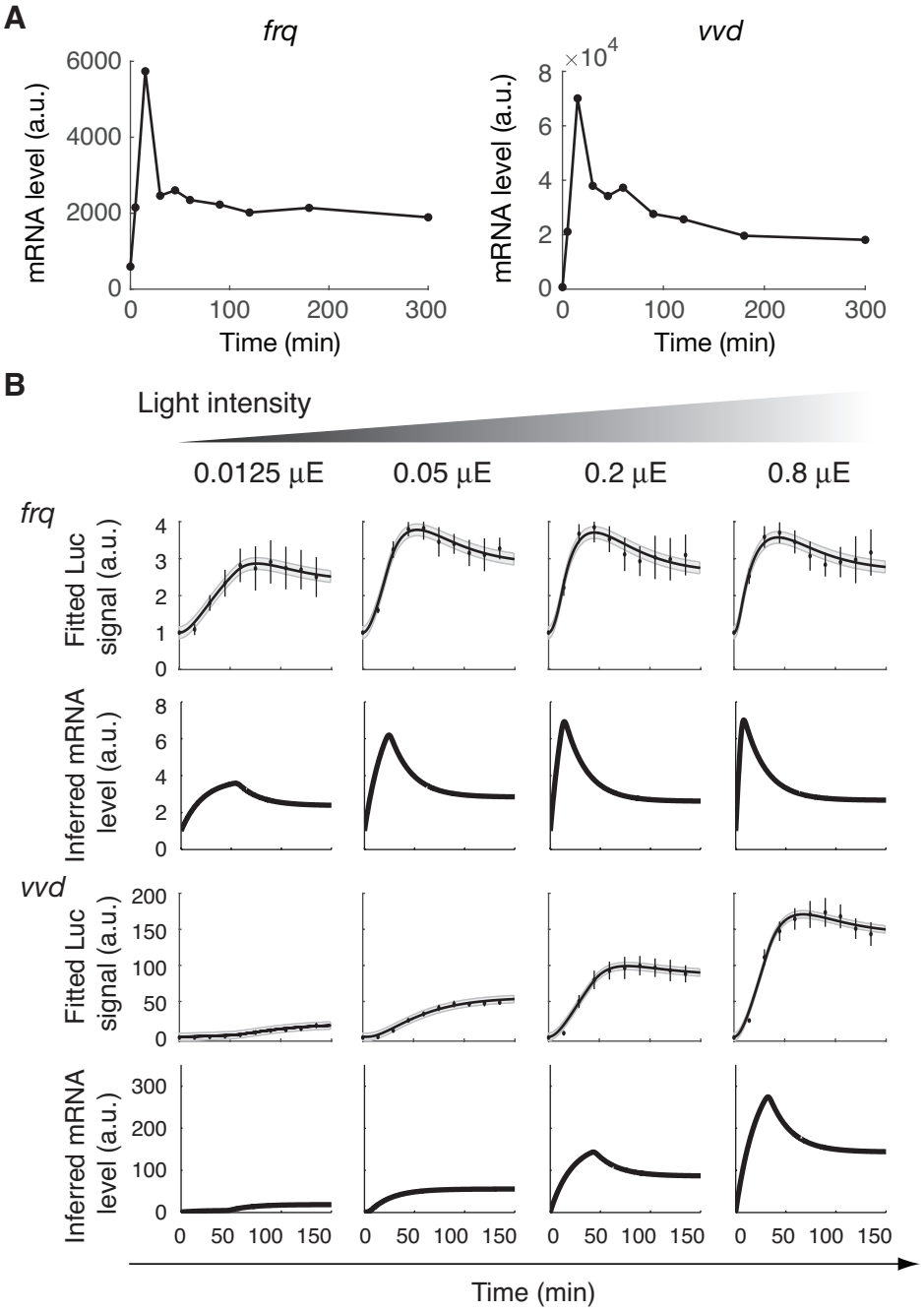

Figure S7. Overshoot in mRNA dynamics under constant light, Related to Figure 4 and STAR Methods. (A) Dynamics of *frq* and *vvd* mRNA induced by constant high light intensity, quantified by RNA-seq (one experiment per time point). (B) Inference of mRNA kinetics from luciferase reporter under constant low light intensities (n = 4) using a model-assisted method. Data are presented as mean ± SEM.

Table S1. Theory predictions on transcriptional regulation at steady state, Related to Figure 2.

Models		Ω	Δ	m_{basal}
FM	RC(τ_{I})	$K_{\mathrm{d}}\frac{\tau_{\mathrm{I}}}{\tau_{\mathrm{A}}+\tau_{\mathrm{I}}+\tau_{\mathrm{R}}}$	$f\frac{\tau_{\mathrm{A}}}{\tau_{\mathrm{A}}+\tau_{\mathrm{I}}+\tau_{\mathrm{R}}}$	0
	RC(τ_{R})	$K_{\mathrm{d}}\frac{\tau_{\mathrm{R}}}{\tau_{\mathrm{A}}+\tau_{\mathrm{I}}+\tau_{\mathrm{R}}}$	$f\frac{\tau_{\mathrm{A}}}{\tau_{\mathrm{A}}+\tau_{\mathrm{I}}+\tau_{\mathrm{R}}}$	0
	TG	$K_{\mathrm{d}}\frac{\tau_{\mathrm{I}}}{\tau_{\mathrm{A}}+\tau_{\mathrm{I}}}$	$f\frac{\tau_{\mathrm{A}}}{\tau_{\mathrm{A}}+\tau_{\mathrm{I}}}$	0
DM	RC	$K_{\mathrm{d}}\frac{\tau_{\mathrm{A}}+\tau_{\mathrm{I}}+\tau_{\mathrm{R}}}{\tau_{\mathrm{A}}}$	$f\frac{\tau_{\mathrm{I}}+\tau_{\mathrm{R}}}{\tau_{\mathrm{A}}+\tau_{\mathrm{I}}+\tau_{\mathrm{R}}}$	$\tau_{\mathrm{mRNA}}f\frac{\tau_{\mathrm{A}}}{\tau_{\mathrm{A}}+\tau_{\mathrm{I}}+\tau_{\mathrm{R}}}$
	TG	$K_{\mathrm{d}}\frac{\tau_{\mathrm{A}}+\tau_{\mathrm{I}}}{\tau_{\mathrm{A}}}$	$f\frac{\tau_{\mathrm{I}}}{\tau_{\mathrm{A}}+\tau_{\mathrm{I}}}$	$\tau_{\mathrm{mRNA}}f\frac{\tau_{\mathrm{A}}}{\tau_{\mathrm{A}}+\tau_{\mathrm{I}}}$
AM	RC	K_{d}	$f\frac{\tau_{\mathrm{A}}}{\tau_{\mathrm{A}}+\tau_{\mathrm{I}}+\tau_{\mathrm{R}}}$	0
	TG	K_{d}	$f\frac{\tau_{\mathrm{A}}}{\tau_{\mathrm{A}}+\tau_{\mathrm{I}}}$	0
EB		K_{d}	f	0

FM: burst frequency modulation; DM: burst duration modulation; AM: burst amplitude modulation. EB: equilibrium-binding model; TG: telegraph model; RC: refractory-cycling model; RC(τ_{I}): refractory-cycling model with TF modulating the $\mathrm{I}\rightarrow\mathrm{A}$ transition; RC(τ_{R}): refractory-cycling model with TF modulating the $\mathrm{R}\rightarrow\mathrm{I}$ transition.

Table S2. Parameter inference for *frq* and *vvd*, Related to Figure 5.

Parameter	Description	Value	Confidence interval
τ_{I}^{frq}	Minimum mean lifetime of inactive *frq* promoter	0.017 min	$(0\ 0.095]$ min
τ_{I}^{vvd}	Minimum mean lifetime of inactive *vvd* promoter	1.7 min	$[1.1\ 3.1]$ min
τ_{R}^{frq}	Mean lifetime of refractory *frq* promoter	46.1 min	$[35.7\ 60.8]$ min
τ_{R}^{vvd}	Mean lifetime of refractory *vvd* promoter	33.4 min	$[15.4\ 65.0]$ min
τ_{A}^{frq}	Mean lifetime of active *frq* promoter	13.8 min	$[10.5\ 16.9]$ min
τ_{A}^{vvd}	Mean lifetime of active *vvd* promoter	17.2 min	$[14.4\ 20.0]$ min
K_{d}^{frq}	Dissociation constant of WCC from *frq* LRE	3548.1 au	$[2437.8\ 4602.6]$ au
K_{d}^{vvd}	Dissociation constant of WCC from *vvd* LRE	2243.9 au	$[1510.1\ 3020.0]$ au
f^{frq}	Transcription initiation rate of *frq* promoter	$18.5\ \mathrm{min}^{-1}$	$[16.1\ 22.4]\ \mathrm{min}^{-1}$
f^{vvd}	Transcription initiation rate of *vvd* promoter	$424.6\ \mathrm{min}^{-1}$	$[306.9\ 669.9]\ \mathrm{min}^{-1}$
τ_{m}^{frq}	Mean lifetime of *frq* mRNA	4.8 min	$[2.2\ 7.9]$ min
τ_{m}^{vvd}	Mean lifetime of *vvd* mRNA	0.017 min	$(0\ 1.3]$ min
v_{wa}	Rate constant of WCC activation by light	$0.16\ \mathrm{min}^{-1}\mu\mathrm{E}^{-1}$	$[0.14\ 0.18]\ \mathrm{min}^{-1}\mu\mathrm{E}^{-1}$
τ_{phos}	Mean lifetime of light form WCC	9.5 min	$[8.2\ 11.0]$ min
τ_{wp}	Mean lifetime of phosphorylated WCC	38.0 min	$[31.0\ 47.0]$ min
τ_{L}	Mean lifetime of stable luciferase protein	635.3 min	$[550.8\ 739.6]$ min
τ_{mL}	Mean lifetime of luciferase mRNA	19.7 min	$[17.1\ 22.6]$ min
η	Factor for luciferase mRNA production rate	2.1	$[1.8\ 2.4]$
$\sigma_{\mathrm{wcc}}^{frq}$	Estimated error of WCC occupancy at *frq* LRE	2.1 au	$[1.5\ 2.9]$ au
$\sigma_{\mathrm{wcc}}^{vvd}$	Estimated error of WCC occupancy at *vvd* LRE	2.5 au	$[1.9\ 3.6]$ au
$\sigma_{\mathrm{mrna}}^{frq}$	Estimated error of *frq* mRNA	0.58 au	$[0.43\ 0.82]$ au
$\sigma_{\mathrm{mrna}}^{vvd}$	Estimated error of *vvd* mRNA	10.1 au	$[7.1\ 14.8]$ au
$\sigma_{\mathrm{L}}^{frq}$	Estimated error of *frq* luciferase	0.19 au	$[0.17\ 0.21]$ au
$\sigma_{\mathrm{L}}^{vvd}$	Estimated error of *vvd* luciferase	0.65 au	$[0.59\ 0.73]$ au
$\sigma_{\mathrm{Lres}}^{frq}$	Estimated error of *frq* luciferase (dose-response)	0.12 au	$[0.11\ 0.13]$ au
$\sigma_{\mathrm{Lres}}^{vvd}$	Estimated error of *vvd* luciferase (dose-response)	0.98 au	$[0.88\ 1.1]$ au
c_{Lres}^{frq}	Scaling factor of *frq* luciferase (dose-response)	1.06	$[1.01\ 1.11]$
c_{Lres}^{vvd}	Scaling factor of *vvd* luciferase (dose-response)	1.69	$[1.64\ 1.74]$
s_{wcc}	Scaling factor of WCC occupancy	0.004 au	$[0.003\ 0.006]$ au
τ_{o}^{frq}	Promoter open time for *frq* (derived from τ_{I}^{frq})	0.16 au	$(0.16\ 0.90]$ au
τ_{o}^{vvd}	Promoter open time for *vvd* (derived from τ_{I}^{vvd})	2.30 au	$[1.5\ 4.2]$ au

Table S3. Sequence of the *frqΔLRE* promoter, Related to Figure 6. Mutagenized nucleotides are bolded and underlined.

gatccgggatagcagagaacctcaatctccacacaagaaatgtctggcctggcactcgtctagcccctgtttcttg
gagggccaacgtatcgagctaacaagttatatccgcgcaagaagatgacgtcataccacgaccgttaagactat
cgtcttggcaccacgaatgaaaaagggtctggacctggccaggcgcggctggccacagctgttttcaggtgaca
ggggcgcagtaccagttgaggagcacctgcgcacgctgtcgagagcgaactgttgcccgtactttgttctagcac
ctgaaagttacagggaccatcgcgggtgctcgcaactgcgctttgggactttccacttacactagtagtgtcaacg
acggacgtttccaaattttgatctctcttgattttcgacatgtttccatcgttcatgactccccgtgtttctcccaagtaaa
tgctgacaaaaccaaactgcgaaactaagtctgtctcagtatctcttagagatgaggagacggcatcgagatcag
acggcaggtggttgggaatggcttgtcacacatcagtcaacattacctctctctctacgtactctagcatttgcacaa
agtctcctttgatatgcccagaaaatctgcagctatagcggatggctgagaagcggatgtttgtcagggtcaacatg
aacttgtactgcatgaattccacttgctgcccttcatcagatccaaacctcaatacctagcatgacggacaactgga
gaaaccgcgaaaaacaggtaccgtcctgtacgatgtgagagaaacaaacctggtgcgccagccgaataagctt
tctttatgtttgttgctgaaaacagaagaatacttggcgatacctgccgacatggtggtctgaatctcaccaccacca
aaaacacaagggctcgcggtcttccgcaggatctcgaatctgttaaaaatgcgagctctccaccaccaccacca
ccaccaccacagagtccatactgtacagccccagggcacacacgtacctatcatgattatgcaaaaccgttaaa
acccttgaaattcgtggagcatttcaacaggtgacaattaagggttcaactccgccgctcgccaaatgcaatatgta
ggtaggggttttccatgtggaaccatggtcgcacgtcggggtactttcagggttcgtaggtcatgtactctgcgcaa
accgttttgtgaaggcattttgggaacacgcaagttggtcgggttgccgtgactccccccttgacttttttcgtgggtga
ggccattcaagtcaagctcgtacccacatccccacaggttccagagtttggccggacaaccagtacgggtgccc
gaggcgtcctgatgccgctgcaagaccgatgacgctgcaaaattgagatctggaggctcaagatactttcggtcg
aagccccaccgccgcgacctcctgtgccacctttccgccaggctgttgtggaaagtcactgcagcgcacccccct
ttgcgagcaatgacgttagaagatgtgggacgttgctcgataggcccaccccgcgtggcgtcaaagtggagccg
cccacaatcctgagcgcagcctgtgatcctgataaccgacaagatgggtgcgaatggaggcattttggggccag
caactgcgctcggagtttccgtccctcacatttttccttggattgcttgcgagtcaggcgcacgtgctctctcgctcg
gtcattgattgatgcggattgccggcgaccatgctgattgattgattgattatgctttggagcgaaccatccggattgt
gctaggtagtgtaagggatttccagacgaggttatgaccgttgcgacgggcggggttgcgttgaaaatctggttac
gaggtcgtcgctcctggttcagagttgccaaagagtgtgagaggccaagtgagctgctggtaggtaggaaactg
cattcatgaggtggagacgacaagcacagatttagacttacccacaacaccatagcaatacatggtgggttaaga
ggatttcaaattttatcgagccgggcggggtgaacaaagcgattcaaggtgttcctggcctctaacaaagaacac
ctgcgctctcttcaccgggcgccgacattgtcggccctgtacgatggcttttggcagaaacatgagggaaaaaa
ccggtcaattggggagatgaagggcgagagctgctggtcatctcctcagcattttgtcgtgagggctttgcggttcg
gacaaagtgagaatcaagttggggaggttgatggatggggagcgggcctacaagtatctcttgatcctctgggga
ccggacgacggctggccaattagacggccgtcgcagaggaccctgaacttttc**ga**tccgct**gc**a**a**cccctgga
acctgggcagtgatgaggatcggggcgattcctgtgcatctgtgggaaagtgagcaagagagcacgacgcgtg
cctctattcgcaaccaacgtaagtatgtgctccggtccagtcccctcgtcccctcctggccctccctccccttttcca
cgccggccccagtctgaatctttacacactccattgcaaaaacggcattggatgaaattatttcgattacccaaact
acacagaaacacacccgcacccgcactcacctgaccgcccgcaaacacacttcgatccggaattcgattgtcg
atgcggccgc

Table S4. Primers used for *frq* and *vvd* hybrid luc_{PEST} constructs, Related to Figure 6.

Primer name	Primer sequence 5'-3'
frq-frqLRE -0.5 lucPEST_fwd	aaagcatgcgcgctctcttcaccgggc
frq-frqLRE -0.5 lucPEST_rev	aaaggcgcgccatcgacaatcgaattccggatc
frq-frqLRE -1.1 lucPEST_fwd	aaagcatgccaatgacgttagaagatgtgggacg
frq-frqLRE -1.1 lucPEST_rev	aaaggcgcgccatcgacaatcgaattccggatc
vvd-frqLRE -1.6 lucPEST_fwd	aaagcatgcagaaagtgtcccccaagttcgc
vvd-frqLRE -1.6 lucPEST_rev	aaaggcgcgccggtgctggttatgagacagtgtgttg
vvd-frqLRE -1.0 lucPEST_fwd	aaagcatgcagacggggcacatgatggg
vvd-frqLRE -1.0 lucPEST_rev	aaaggcgcgccggtgctggttatgagacagtgtgttg
vvd-frqLRE-0.4 lucPEST_fwd	aaagcatgcgcatcccaaacacccctgg
vvd-frqLRE-0.4 lucPEST_rev	aaaggcgcgccggtgctggttatgagacagtgtgttg
vvd-frqLRE -0.2 lucPEST_fwd	aaagcatgcaacctcatagcctttcttcctttgc
vvd-frqLRE -0.2 lucPEST_rev	aaaggcgcgccggtgctggttatgagacagtgtgttg
vvd-frqCorePromTSS lucPEST_fwd	aaagcatgccgcaaccaacgtaagtatgtgctc
vvd-frqCorePromTSS lucPEST_rev	aaagcggccgcaaagattcagactggggccg
Mut-SphI-into-vvd-lucPEST_fwd	atctcgatcgacggcatgccggcgctcaatcccaa
Mut-SphI-into-vvd-lucPEST_rev	ttgggattgagcgccggcatgccgtcgatcgagat

Table S5. Primers and probes used for qRT-PCR and ChIP-qPCR, Related to Figure 6.

Primer name	Forward primer sequence 5'-3'
	Reverse primer sequence 5'-3'
	TaqMan probe sequence 5'-3' or Roche UPL probe
	Description
frq_orf	ttgtaatgaaaggtgtccgaaggt ggaggaagaagcggaaaacg acctcccaatctccgaactcgcctg *frq* mRNA
vvd_orf	acgtcatgcgctctgattctg aaaagcttccgaggcgtaca cgacctgaagcaaaaagacacgcca *vvd* mRNA
28S_rRNA	gaacaacagggattgcccta ggactcagaaggtgcctcac tgaaatctggcttcggcccg normalisation of mRNA and ChIP
frq_LRE	tctcttgctcactttcccacag gcagaggaccctgaacttttc ccgctcgatcccctggaacctg ChIP-PCR (WC-2 ChIP)
vvd_LRE	tggatggcagtgtagaatgg gtccctcgatggtttagcag ctgcgatcggtcagcatcgc ChIP-PCR (WC-2 ChIP)